DEVELOPMENT OF AN IN-SITU METHOD OF PH MEASUREMENT WITH CALIBRATION FOR USE UNDER HIGH HYDROSTATIC PRESSURES

by

TRISTIN LEIGH THOMPSON

(Under the Direction of Jose Reyes De Corcuera)

ABSTRACT

Though pressure has been used in food processing for over 30 years, there is still no clear choice when determining the pH of a sample under high hydrostatic pressure. A cell design is proposed for use as a pH sensing device that functions under high pressure. The design mimics the glass pH electrode in that it uses a working and reference electrode to measure the potential of a solution. Calibration of the sensor under high pressure relied on the use of two baroresistant buffers at pH 4 and 7. The sensor did show a change in voltage with pH under pressure, but showed reduced sensitivity as pressure increased and low precision in measured values. A baroresistant buffer was developed at pH 7, but was not at pH 4. A second baroresistant calibration buffer and improvement in the sensor's sensitivity are necessary before the design can be used in analytical experiments.

INDEX WORDS: HIGH PRESSURE, PH, HIGH HYDROSTATIC PRESSURE, BARORESISTANT BUFFER, ISOSBESTIC

DEVELOPMENT OF AN IN-SITU METHOD OF PH MEASUREMENT WITH CALIBRATION FOR USE UNDER HIGH HYDROSTATIC PRESSURES

by

TRISTIN LEIGH THOMPSON

BS, University of Georgia, 2014

A Thesis Submitted to the Graduate Faculty of The University of Georgia in Partial Fulfillment of the Requirements for the Degree

MASTER OF SCIENCE

ATHENS, GEORGIA

2016

DEVELOPMENT OF AN IN-SITU METHOD OF PH MEASUREMENT WITH CALIBRATION FOR USE UNDER HIGH HYDROSTATIC PRESSURES

by

TRISTIN LEIGH THOMPSON

Major Professor:	Jose Reyes De Corcuera
Committee:	Rakesh Singh
	Geoffrey Smith

Electronic Version Approved:

Suzanne Barbour
Dean of the Graduate School
The University of Georgia
May 2016

DEDICATION

I would like to dedicate this thesis to my grandmother, JoAnn Thompson. Though I received relatively unconditional support from my family in my decision to study Food Science, she was able to make it possible for me while funding was not secured. I am incredibly grateful that I was able to stay in Georgia while continuing my studies. Things would not have been the same otherwise.

ACKNOWLEDGEMENTS

Completing my thesis and the work in lab that came before it took a lot of focus, determination, and most notably, support. I would like to thank all those who helped along the way when I ran into issues that seemed too large to overcome, including my fellow lab mates and graduate students. Finally, a thank you goes out to Dr. Reyes for providing me with an interesting problem to solve and the materials to do so.

TABLE OF CONTENTS

Page

ACKNOWLEDGEMENTS v

LIST OF TABLES viii

LIST OF FIGURES ix

CHAPTER

1 Introduction 1

Background 1

Literature Review on High Pressure pH Measurements 5

Research Proposal 8

References 10

2 Preparation of Baroresistant Buffers 14

Introduction 14

Materials and Methods 16

Results 22

Discussion 28

Conclusion 32

References 55

3 Development and Testing of a High Pressure pH Probe Assembly 57

Introduction 57

Materials and Methods 59

Discussion 71

Conclusion 72

References 85

APPENDICES

A Code for Modeling Data 88

LIST OF TABLES

Page

Table 2.1: Fitting Parameters and ΔpKa/ΔP for Indicator Dyes.....43

LIST OF FIGURES

Page

Figure 2.1: High Pressure Optical System 34

Figure 2.2: Visible Spectra of Methyl Orange at 25 °C at Varying pH Values 35

Figure 2.3: Delocalization of Charge in Acidic Form of Methyl Orange 36

Figure 2.4: Visible Spectra of Bromophenol Blue at 25 °C at Varying pH Values 37

Figure 2.5: Visible Spectra of Bromocresol Green at 25 °C at Varying pH Values 38

Figure 2.6: Visible Spectra of Phenol Red at 25 °C at Varying pH Values 39

Figure 2.7: Ratiometric Absorbance of Bromophenol Blue vs Solution pH at 25, 45, and 65 °C 40

Figure 2.8: Ratiometric Absorbance of Bromocresol Green vs Solution pH at 25, 45, and 65 °C 41

Figure 2.9: Ratiometric Absorbance of Phenol Red vs Solution pH at 25, 45, and 65 °C 42

Figure 2.10: Change in pH with Pressure for Phenol Red 44

Figure 2.11: Change in pH with Pressure for Bromophenol Blue 45

Figure 2.12: Effect of Pressure on the Calculated pH for Tris 0.6905 Molar Fraction at 25 °C 46

Figure 2.13: Tris/tricarballylate Molar Fraction vs $\Delta pH/\Delta P$ at 25 °C 46

Figure 2.14: Effect of Pressure on the Calculated pH for Tris 0.86 Molar Fraction at 25 °C 47

Figure 2.15: Effect of Pressure on the Calculated pH for 100 mM Tris Buffer at 25 °C ..47
Figure 2.16: Tris/tricarballylate Molar Fraction vs ΔpH/ΔP at 45 °C 48
Figure 2.17: Tris/tricarballylate Molar Fraction vs ΔpH/ΔP at 65 °C 48
Figure 2.18: Effect of Pressure on the Calculated pH for Tris 0.76 Molar Fraction at 45 °C 49
Figure 2.19: Effect of Pressure on the Calculated pH for Tris 0.75 Molar Fraction at 65 °C 49
Figure 2.20: Methylpiperazine/Acetate Molar Fraction vs. ΔpH/ΔP at 25 °C 50
Figure 2.21: Effect of Pressure on the Calculated pH for 100 mM Acetate at Acidic and Neutral pH.....50
Figure 2.22: Effect of Pressure on the Calculated pH for 100 mM Succinic Acid at 25 ° C 51
Figure 2.23: Effect of Pressure on the Calculated pH for 100 mM Citrate at Acidic and Neutral pH.....51
Figure 2.24: Acetate Molarity vs ΔpH/ΔP at 25 °C.....52
Figure 2.25: Effect of Pressure on the Calculated pH for 100 mM Acetate at 25 °C.....52
Figure 2.26: Effect of Pressure on the Calculated pH for 100 mM Acetate at 45 °C.....53
Figure 2.27: Effect of Pressure on the Calculated pH for 100 mM Acetate at 65 °C.....53
Figure 2.28: UV-vis of Water in Cuvette under Pressure.....54
Figure 3.1: High pressure electrochemical system 74
Figure 3.2: Potential over Time of ZrOx Electrodes against Ag/AgCl Reference Electrode in 3M KCl 75

Figure 3.3: ZrOx Potential against Ag/AgCl Reference Electrode in 3M KCl at 25°C in pH calibrations buffers 4.01, 7, and 10.01 76
Figure 3.4: Potential of IrOx Electrodes against Ag/AgCl Reference Electrode at 25°C using pH Calibration Buffers 4.01, 7, and 10.01 77
Figure 3.5: Potential of IrOx against Ag/AgCl across pH 2-10 at 25 °C 78
Figure 3.6: First Prototype 79
Figure 3.7: Prototype 2 80
Figure 3.8: Prototype 3 80
Figure 3.9: Ag/AgCl Reference Electrode 81
Figure 3.10: Silicone Putty Molds Used for Electrode Cap Production 81
Figure 3.11: Finished prototype 82
Figure 3.12: Potential of IrOx Electrode vs Internal and External Ag/AgCl Reference Electrode 83
Figure 3.13: Cell Calibration at 25 °C from 0.1 to 400 MPa Using Baroresistant Calibration Buffers 83
Figure 3.14: pH Sensor Sensitivity vs Pressure 84
Figure 3.15: Change in pH Sensitivity as Electrodes were Altered 84

CHAPTER 1

INTRODUCTION

Background

As consumers in developed and developing countries are becoming more conscientious about what they eat, pressure has fallen on food processors to simplify the ingredients list on nutrition labels through limited use of chemical preservatives and antimicrobials along with use of natural flavorings instead of artificial flavorings. Without the use of chemical preservatives and antimicrobials, reduction of microbial load through processing becomes crucial to extending the shelf-life when considering food safety (Toepfl et al., 2006). Because heat treatments can cause production of off-flavors in fresh flavor profile products, nutrient degradation, and other undesirable changes, application of high hydrostatic pressure (HHP) has been studied for several decades as a non-thermal method of pasteurization. Though HHP is currently approved for processing of several food items, research on the topic continues to find new possible applications of HHP in food processing.

Food processors are also seeking ways to reduce energy use for economic and environmental reasons (Toepfl et al., 2006). Though the capital cost for high pressure generators can range between $650,000 and $2.6 million depending on desired capacity, operating costs can decrease due to lower energy usage, reduced processing times, and

less processing steps when compared to traditional thermal treatments. For example, the sterilization of a can using thermal means has a specific energy input of 300 kJ/kg, while the sterilization using combined thermal and high pressure treatments has a specific energy input of 242 kJ/kg when assuming a heat recovery rate of 50% in both processes. This decrease in energy input can be attributed to the adiabatic heating that occurs as fluids are compressed and experience internal friction. As HHP processing becomes more widespread and production of equipment increases, initial equipment costs will decrease (Martínez-Rodríguez et al., 2012).

HHP processing is a pressurizing treatment used to process many commercial products such as cheese, jams, fresh fruit and vegetables, guacamole, milk, salsa, frozen meals, orange juice, and ham. Typical pressures range from 300-700 MPa which is applied instantaneously and uniformly to the product regardless of physical parameters such as density or shape, as explained by the isostatic principle (Min et al., 2007). As the sample is compressed, adiabatic heating occurs evenly throughout the sample (Kadam et al., 2012). The intrinsic adiabatic heating that occurs during pressurization along with increased sensitivity to thermal treatments allows for less thermal energy to be input into the system to achieve the same inactivation of microorganisms as compared to traditional thermal processing. Significant inactivation at pressures of 400 MPa and above without thermal treatment was also observed (Toepfl et al., 2006). Pressure inactivates microorganisms causing cell injury by denaturing proteins among other effects (Kadam et al., 2012). Several review papers included here discuss the validity of high pressure

pasteurization and will therefore not be discussed in detail (Demazeau and Rivalain, 2011; Kadam et al., 2012; Toepfl et al., 2006).

HHP processing is currently being researched by several groups for nutritional effects on berry juices (Altuner and Tokuşoğlu, 2013), sensory changes in beer and wine (Buzrul, 2012), and potential for processing fruit and vegetable products with varying acidity (Guerrero-Beltrán et al., 2005). HHP processing is a desirable alternative to thermal treatments as it can significantly reduce microbial load while retaining the nutritional and sensory qualities of the fresh product (Demazeau and Rivalain, 2011). High pressures typically experienced during processing do not affect covalent bonds, therefore the low molecular weight components contributing to the nutritional and sensory characteristics of the product are unaffected. Non-covalent bonds, such as hydrophobic interactions and hydrogen bonding, are affected however leading to changes in protein tertiary structure and functionality (Kadam et al., 2012).

Equilibrium reactions are temperature and pressure dependent. According to Le Châtelier's principle, any system at equilibrium whose equilibrium is disrupted will react in an opposite fashion to restore equilibrium. Gaseous systems under pressure will undergo a shift to minimize the number of moles present in the system while aqueous systems will shift towards the larger decrease in molar volume (McQuarrie, 1997). A robust mathematical model has not yet been developed to explain the change in thermodynamic equilibrium constants with change in pressure as detailed by Stippl, Delgado, and Becker, (2005), but there are some that agree enough with empirical measurements to be considered useful. Equation 1.1 shows the pressure dependence of

the equilibrium constant as derived from the pressure dependence of the dielectric permittivity where *K* represents the equilibrium constant at standard pressure (0) and at elevated pressure (*P*), b is a constant (=9.2810^{-5} bar^{-1}), and ΔV_0 is the molar volume change at standard pressure upon ionization (El'yanov and Hamann, 1975). This equation is shown to begin deviating from empirical measurements of the equilibrium constants at pressures exceeding 600 MPa, though still retains the same character and relative proximity to empirical measurements up through 1200 MPa (Stippl et al., 2005).

$$RTln\left(\frac{K_P}{K_0}\right) = -\frac{\Delta V_0 P}{1+bP} \qquad (1.1)$$

Ionization reactions are favored when solutions undergo an increase in pressure due to the electrostriction of water molecules surrounding the ions, causing a net decrease in volume. This includes the deprotonation of acids (Lown et al., 1968). Because the acids will be deprotonated, the proton concentration will increase causing a decrease in pH. This has been observed experimentally up to 100 MPa in seawater by Culberson & Pytkowicz (1968). Pressure not only affects the pH of a solution, but also the effect that the pH has on the solution. Changes in pH have been linked to changes in gelification, enzyme activities, chemical reactions (like Maillard browning), the denaturing of proteins, and the survival rate of microorganisms, all of which are important to consider when processing food (Stippl et al., 2005).

Over 100 papers have been published in the past 10 years on the electrical conductivity of solutions at high pressure and several valid electrochemical cell designs have been tested up to 2,700 MPa, but there is still not a clear, reliable choice when measuring pH under high pressure conditions (Debora et al., 2004). Several fields, such

as the food industry, pharmaceutical industry, oil refining, and deep-sea research, would benefit from the manufacturing of a robust pH sensing device that can withstand higher pressures and the complex matrices of biological, environmental, and food-based samples than currently available. Once such a laboratory pH probe prototype is developed, the next step will be to modify it for on-line measurements.

Literature Review on High Pressure pH Measurements

Old Research and Existing Technology

Historically, conventional pH measurements have been made using glass electrodes. Improvements upon the original design have led to modifications that have a workable temperature range of -25 to 130 °C with different models. They also have good Nernstian behavior, long term stability, low detection limits, and are insensitive to redox systems (Vonau and Guth, 2006). However, the glass membrane lends these electrodes to be very fragile and therefore unusable under high pressures or within a food processing facility due to risk of broken glass in the product.

Field-effect transistors have been used for several decades in the electronics industry and have been adapted for use in analytical chemistry. Application of an ion-selective membrane across the gate allows for only selected ions to be measured and makes an ion-selective field-effect transistor (ISFET) (Kress-Rogers, 1991). ISFETs are able to be miniaturized, have faster response times than glass electrodes, and are less fragile that glass electrodes making them a great alternative. However, it is prudent that the device be sealed from solution with an ion-permeable membrane as they are sensitive to water (Skoog et al., 1998). Research by Le Bris & Birot has shown no loss of sensitivity in the

pH-ISFET after operating at 3 MPa for 43 hours (1997). Unfortunately, no other research was found on the performance of pH-ISFET sensors at more elevated pressures.

Indicator dyes have long been used to visually show the change of pH in a solution, particularly when performing titrations without a pH meter. A more analytical approach has been to correlate the absorbance at a specific wavelength with the proton concentration in the solution. This method has the limitation of only being applicable at pH values near the pKa of the dye itself. By using multiple indicator dyes in the test solution, Stippl, Delgado, and Becker, (2004) were able to measure pH values up to pressures of 450 MPa with an error of 0.24 pH units. Temperature was not accounted for and this method is limited to translucent liquids without strong coloring that would interfere with the absorbance spectrum. This technique has also been studied using fluorescent dyes which allows for stronger colored solutions to be analyzed provided there is little to no fluorescence in the product (Salerno et al., 2007). Use of the UV-vis absorbance or fluorescence spectra in the determination of pH is useful when considering high pressure, but overall does not show significant potential as a routine pH sensing method in food industry applications because adding such indicators to foods would be very expensive and result in adulterated products.

Current Research

Samaranayake & Sastry (2010) used modified conductivity measurements to determine pH at pressures up to 784 MPa. They designed a conductivity cell made of flexible tubing to allow pressure to be transmitted to the test solution. Each end of the cell had a lead wire that served as an electrode. Ion-selective membranes were placed in the

middle of the cell to allow only the flow of protons through the cell when a voltage was applied, allowing the measured current to be related to the proton concentration. Extensive calculations and correction factors were determined to account for changes in the cell constant due to pressurization. The pH of several biological buffers was measured up to 784 MPa and compared to the theoretical values calculated using reaction volume based methodologies. Measured pH values for acetic acid buffer showed a shift in pH with pressure ($\Delta pH/\Delta P$) of -0.03 pH/100 MPa while the theoretical value using El'Yanov's equation is -0.12 pH/100 MPa. At the highest pressure point of 784 MPa, the difference was 0.72 pH units. Their results also showed little agreement with other published data which gave $\Delta pH/\Delta P$ values of -0.2 pH/100 MPa(Hayert et al., 1999). Because the theory of high-pressure chemistry is still not well understood nor is a comprehensive theory developed, the results must be compared to other experimental data.

Recently, numerous studies have been published discussing the use of metal oxide electrodes in oil drilling mud (Lorant et al., 2013), elevated temperatures (Pan and Seyfried, 2008), and high pressures (Zhang et al., 2008). Metal oxide electrodes have a strong preference for hydrogen ions and when made using current techniques, show a pH response of near or above the ideal Nernstian value of -59.16 mV/pH (Vonau and Guth, 2006). Metal oxide electrodes show promise for high pressure applications due to their robust construction and good response across a defined pH range, depending on the metal oxide and method of production.

Iridium oxide has been explored as a possible pH electrode. It has been shown to have a linear response across a wide pH range of 2-10, a fast and stable response, and does not require pretreatment like glass electrodes (Kurzweil, 2009). Initial findings showed a very stable electrode with little drift allowing for less frequent calibration at ambient temperature and pressure when used in conjunction with a standard Ag/AgCl reference electrode (Wang et al., 2002). The iridium oxide electrode was tested at higher temperatures and pressures by Pan and Seyfried (2008), and revealed possible structural changes to the electrode when tested at 175 °C and 25 MPa. The electrode showed good agreement with calculated pH values and a near-theoretical slope during calibration when the temperature was reduced and the pressure held constant (Pan and Seyfried, 2008). Typically, food processing temperatures do not reach 175 °C so this deviation is not of concern.

Research Proposal

A large gap of knowledge and technology exists, as a practical method to accurately determine the pH change of a food product during application of HHP is not currently available. No equations that reasonably predict $\Delta pH/\Delta P$ are currently capable of doing so for a complex matrix as found in food products and only two papers are currently published on the effect of pressure on pH in food products. This knowledge is essential, not just for food quality concerns, but also for those of safety. The pH of a solution is one of several major factors when determining microbial inactivation and a better understanding of how this factor changes under new processing techniques is crucial for

determining the processing conditions that make a product safe when processed under HHP.

At this time, there is no clear choice for taking pH measurements of a solution under high hydrostatic pressure. Our objective will be to develop a pH sensing device that functions under high hydrostatic pressure. A set of baroresistant pH standard buffers at pH 4 and 7 will be used to calibrate the pH sensor under applied pressures.

References

Altuner, E.M., Tokuşoğlu, Ö., (2013). The effect of high hydrostatic pressure processing on the extraction, retention and stability of anthocyanins and flavonols contents of berry fruits and berry juices. International Journal of Food Science & Technology, n/a-n/a.

Buzrul, S., (2012). High hydrostatic pressure treatment of beer and wine: A review. Innovative Food Science & Emerging Technologies 13, 1-12.

Culberson, C., Pytkowicz, R.M., (1968). Effect of Pressure on Carbonic Acid, Boric Acid, and the pH in Seawater. American Society of Limnology and Oceanography, p. 403.

Debora, G., Nathan , S.L., Richard , G.C., (2004). Electrochemistry at High Pressures: A Review. Electroanalysis 16(10), 789.

Demazeau, G., Rivalain, N., (2011). The development of high hydrostatic pressure processes as an alternative to other pathogen reduction methods. Journal of Applied Microbiology 110(6), 1359-1369.

El'yanov, B.S., Hamann, S.D., (1975). Some quantitative relationships for ionization reactions at high pressures. Australian Journal of Chemistry 28(5), 945.

Guerrero-Beltrán, J., Barbosa-Cánovas, G., Swanson, B.G., (2005). High Hydrostatic Pressure Processing of Fruit and Vegetable Products. Food Reviews International 21(4), 411-425.

Hayert, M., Perrier-Cornet, J.-M., Gervais, P., (1999). A simple method for measuring the pH of acid solutions under high pressure. The Journal of Physical Chemistry A 103(12), 1785-1789.

Kadam, P.S., Jadhav, B.A., Salve, R.V., Machewad, G.M., (2012). Review on the high pressure technology (HPT) for food preservation. Journal of Food Processing and Technology 3(1), 135-135.

Kress-Rogers, E., (1991). Solid-state pH sensors for food applications. Trends in food science & technology 2(12), 320-324.

Kurzweil, P., (2009). Metal Oxides and Ion-Exchanging Surfaces as pH Sensors in Liquids: State-of-the-Art and Outlook. Sensors (14248220) 9(6), 4955-4985.

Le Bris, N., Birot, D., (1997). Automated pH-ISFET measurements under hydrostatic pressure for marine monitoring application. Analytica Chimica Acta 356, 205-215.

Lorant, S., Bohnke, O., Breviere, J., Bohnke, C., (2013). All-Solid-State pH Sensor Used in Oil Drilling Mud. Electroanalysis 25(1), 223-229.

Lown, D.A., Thirsk, H.R., Wynne-Jones, L., (1968). Effect of pressure on ionization equilibria in water at 25°C. Transactions of the Faraday Society 64, 2073.

Martínez-Rodríguez, Y., Acosta-Muñiz, C., Olivas, G.I., Guerrero-Beltrán, J., Rodrigo-Aliaga, D., Sepúlveda, D.R., (2012). High Hydrostatic Pressure Processing of Cheese. Comprehensive Reviews in Food Science & Food Safety 11(4), 399-416.

McQuarrie, D.A.S.J.D., (1997). *Physical chemistry : a molecular approach*. University Science Books, Sausalito, Calif.

Min, S., Sastry, S.K., Balasubramaniam, V.M., (2007). In situ electrical conductivity measurement of select liquid foods under hydrostatic pressure to 800MPa. Journal of Food Engineering 82, 489-497.

Pan, Y., Seyfried, W., (2008). Experimental and Theoretical Constraints on pH Measurements with an Iridium Oxide Electrode in Aqueous Fluids from 25 to 175 °C and 25 MPa. Journal of Solution Chemistry 37(8), 1051-1062.

Salerno, M., Ajimo, J.J., Dudley, J.A., Binzel, K., Urayama, P., (2007). Characterization of dual-wavelength seminaphthofluorescein and seminapthorhodafluor dyes for pH sensing under high hydrostatic pressures. Analytical Biochemistry 362, 258-267.

Samaranayake, C., Sastry, K., (2010). In Situ Measurement of pH Under High Pressure. Journal of Physical Chemistry B 114(42), 13326-13332.

Skoog, D.A., Holler, F.J., Nieman, T.A., (1998). *Principles of instrumental analysis*. 5th ed.Philadelphia : Saunders College Pub. ; Orlando, Fla. : Harcourt Brace College Publishers, c1998.

Stippl, V.M., Delgado, A., Becker, T.M., (2004). Development of a method for the optical in-situ determination of pH value during high-pressure treatment of fluid food. Innovative Food Science and Emerging Technologies 5, 285-292.

Stippl, V.M., Delgado, A., Becker, T.M., (2005). Ionization equilibria at high pressure. European Food Research & Technology 221(1/2), 151.

Toepfl, S., Mathys, A., Heinz, V., Knorr, D., (2006). Review: Potential of High Hydrostatic Pressure and Pulsed Electric Fields for Energy Efficient and

Environmentally Friendly Food Processing. Food Reviews International 22(4), 405-423.

Vonau, W., Guth, U., (2006). pH Monitoring: a review. Journal of Solid State Electrochemistry 10(9), 746.

Wang, M., Yao, S., Madou, M., (2002). A long-term stable iridium oxide pH electrode. Sensors & Actuators: B. Chemical 81, 313-315.

Zhang, R.H., Zhang, X.T., Hu, S.M., (2008). Zr/ZrO2 sensors for in situ measurement of pH in high-temperature and -pressure aqueous solutions. Analytical Chemistry 80(8), 2982-2987.

CHAPTER 2

PREPARATION OF BARORESISTANT BUFFERS

Introduction

Buffers are solutions that contain conjugate weak acid/base pairs and are used commonly to prevent large fluctuations in pH of a solution. Enzymatic reactions have a maximum reaction rate at an optimal pH and enzymes are active within a limited pH range. Microorganisms have specific pH ranges which they can live within as well. As high hydrostatic pressure (HHP) becomes a more prominent means of food processing, control of pH during pressurization will be critical to maintaining control of a system's reactions and equilibria.

When HHP is applied to an equilibrium system, the equilibrium of the system favors reactions with negative reaction volumes. Ionization reactions in particular are favored under HHP due to electrostriction around the formed ions leading to a large negative reaction volume. As pressure is increased, the pKa (log(K)) is increased or has a basic shift, Eq. 2.1 (Lown et al., 1968). K is the equilibrium constant for a reaction. This leads to increased dissociation of hydrogen ions and a negative reaction volume. This equation has been shown to be valid for calculations up to 200 MPa as changes in pK are calculated using compressibility and volume change values at ambient pressure.

Accurate calculations at higher pressure require the dependence of the reaction volume change with pressure as the relationship is not linear (Stippl et al., 2005).

$$pK_p = pK_1 + \frac{P\Delta\overline{V_1^0}}{2.303RT}\left(1 - \frac{P}{9300}\right) \qquad (2.1)$$

Where pK_p is the pKa at pressure P, pK_1 is the pKa at ambient pressure in bars, R is the gas constant, and T is absolute temperature in Kelvin.

When considering equilibria with respect to charge changes, ionization reactions with no formal charge should also be considered. The ionization of Tris buffer is shown in Reaction I. No change in formal charge occurs on either side of the equilibrium reaction, therefore a small reaction volume change occurs. The relationship between reaction volume and the equilibrium constant is shown in Eq. 2.2. Negative reaction volumes are expected when the equilibrium constant increases with pressure and positive reaction volumes are expected with decreases in K. The overall magnitude of the reaction volume change is directly correlated to the change in K, so for reactions similar to the ionization of Tris buffer, little change in K is expected which leads to little change in pH. The change in the pKa of Tris buffer under an applied pressure of 650 MPa showed a decrease of 0.2 pH units (Nueman Jr. et al., 2010).

Reaction I

$$TrisH^+ \leftrightarrow Tris + H_3O^+$$

$$\Delta\overline{V_1} = -RT\frac{\partial K_a}{\partial P} \qquad (2.2)$$

Pressure studies on acetate, citrate, phosphate, potassic, and Good's buffers have shown both positive and negative values indicating that not all buffers experience an acidic pH shift due to pressure. This would allow for the theory that a combination of two buffers with opposing shifts in pH with pressure would essentially cancel out leaving a buffer with minimal shift in pH under pressure (Quinlan and Reinhart, 2005). A set of baroresistant buffers were developed by Quinlan at near neutral pH values for work in biochemical experiments, but calibration requires at least two points and baroresistant buffers at pH 4 and 10 have not yet been developed. This approach of mixing buffers with opposite $\Delta pH/\Delta P$ was used to craft a set of pH calibration buffers with minimal change in pH under pressure at typical calibration points pH 4 and pH 7. The objective of the research reported in this chapter is to develop a set of baroresistant buffers for use in calibrating a high pressure pH probe for use in food pressure studies. Development of a baroresistant buffer at pH 10 was unnecessary as the pH of the majority of foods consumed is between 4 and 7.

Materials and Methods

Materials

Solutions of Bromophenol Blue pKa = 3.94 (Sigma Aldrich, ACS reagent grade), Methyl Orange pKa 3.4 (Fisher, reagent grade), and Phenol Red pKa 7.9 (Fisher, reagent grade) were prepared in distilled water to a final concentration of 0.1% w/v. A solution of Bromocresol Green pKa 4.7 (Acros Organics, reagent grade) was prepared to a final concentration of 0.04% w/v in distilled water. Solutions were stored at 4 °C in amber

bottles until needed. Indicator dyes were chosen near the pH values of interest, 4 and 7, and when possible, the health hazards were minimized as well.

Acetate buffers were prepared from sodium acetate trihydrate (Fisher, ACS grade) and glacial acetic acid (Fisher, ACS grade). Citric acid and succinic buffers were prepared from anhydrous citric acid and succinic acid (Fisher, reagent grade). n-Methylpiperazine at 100 mM was prepared from stock solution (Fisher, 99+%) using ultra-filtered, deionized water and the pH was adjusted using 1M HCl. Tris buffer at 100 mM was prepared from ultra-pure Tris in free-base form (Sigma Aldrich, >99.9%) and tricarballylate buffer was prepared from tricarballylic acid in free acid form (Sigma Aldrich, 99%).

High Pressure Optical System

Optical measurements at HHP were made using the equipment shown in Figure 2.1a-b. The high pressure system consisted of a manual high pressure generator from High Pressure Equipment Company (Erie, PA, USA) model #31-5.75-75. Two high pressure needle valves model #A12513 controlled the flow of oil (the pressurizing medium) throughout the system. A pressure gauge from Astra Products (Ivyland, PA, USA) was attached to the system using a connector from High Pressure Equipment Company model #A12381. This allowed for online measurement of applied pressure in 5 MPa increments up to 700 MPa. A connector was also used to provide a connection to the optical vessel. A high pressure optical vessel was purchased from Unipress Equipment (Warszawa, Poland) model U103. The high pressure generator works by pulling an internal piston out which draws in oil from the reserve. The valve that connects

the reserve is then closed. As the piston is pushed back into the generator, the oil is compressed which leads to an increase in pressure throughout the system.

An Ocean Optics light source model DH-2000-BAL and spectrometer model USB2000+ (Dunedin, FL, USA) were connected to the high pressure optical cell using optic fibers. A Fisher Scientific water bath model Isotemp 4100 was attached to the optical cell to allow for thermal control during experiments. Cylindrical quartz cuvettes with moveable caps on each end allowed for pressure to be transmitted to the sample during pressurization. Cuvettes were filled so as to avoid any air bubbles by adding solution at an angle and twisting the cuvette to fill the bottom. Solution was added to form a meniscus at the top of the cuvette and the second cap was added to close the cuvette. Once the cuvette was placed in the optical cell, oil was added to the cell to ensure no air remained once the lid was screwed on. Weep holes in the lid allowed for trapped air to escape during tightening. Once closed, the sample was pressurized by manually turning the wheel that is connected to the generator. Once at set pressure, five minutes were given for both thermal and pressure equilibrium to occur before recording the spectrum. This waiting period was based on measuring the internal temperature using an attached thermocouple. Pressure equilibrium is assumed instantaneous due to the instant and uniform application of applied pressure in a system. The system was then depressurized prior to opening the optical cell and testing a new sample.

Indicators Spectra and Solution pH

Spectra-pH Correlation

This set of experiments was based on previous work developing baroresistant buffers in the physiological pH range (Quinlan and Reinhart, 2005; Tomlin, 2011). A set of solutions with pH values ranging from plus or minus two pH units around the pKa of the indicator dyes were prepared using 50 mM phosphate buffer and the addition of HCl or NaOH to adjust to the desired pH. PH measurements of the samples were made at a constant temperature of 25 °C by using a larger beaker full of water as an insulating jacket. An aliquot of each solution was transferred to a test tube and stock phenol red solution was added to a final concentration of 0.0015% w/v. A microplate reader model S1A from Biotek (Winooski, Vermont, USA) was used to record the UV-vis spectra of the samples in triplicate with path length correction to report absorbance equivalent to a path length of 1 cm. The microplate reader software was set to maintain an internal temperature of 25 °C during UV-vis measurement. Calibration for bromophenol blue, bromocresol green, and methyl orange was performed using the same procedure as above with the following exceptions. Samples were prepared from 100 mM acetate buffer solution and dye solution was added at a concentration of 0.0015% w/v, 0.02% w/v, and 0.001% w/v of solution, respectively.

Adjustments for the above procedures for calibration at 45 and 65 °C included warming the buffer solution in a water bath for 15 minutes to the set temperature, or until thermal equilibrium. Then, the beaker holding the buffer was wrapped in aluminum foil and kept on a hot plate while adjusting the pH and taking samples. A piece of cardboard

was used as insulation from the hot plate when the solution temperature increased past the set point. Aliquots of each sample taken during production were allowed to cool to room temperature prior to pipetting 5 mL of each sample to account for heat-induced volume changes. UV-vis measurements for samples at 45 °C were still performed in the plate reader with an incubation temperature of 45 °C. Spectra of samples at 65 °C were taken using the high pressure optical vessel which was thermally controlled with a water jacket attached to an external water bath set at 65 °C, as seen in Figure 2.1. The optical measurements were made using the Ocean Optics spectrometer and light source with both hydrogen and deuterium lamps on.

All spectra collected were used to prepare a calibration curve relating the spectra of the indicator dye to the solution's pH at each temperature tested. This calibration relied on taking the ratio between the absorbance at a peak against the absorbance at an isosbestic point (a wavelength where the absorbance does not change with changes in pH). By taking the ratio of the absorbance at the analytical peak and the absorbance at the isosbestic point, a ratiometric absorbance can be obtained. This method gives superior results compared to other spectral analysis methods by accounting for changing cell geometry, dye concentration, and refractive index due to pressure (Stippl et al., 2004) and allowed construction of calibration curves of pH vs. ratiometric absorbance. The correlation equation modeled the ratiometric absorbance of the dye against solution pH and had a logistic form. This allowed for calculation of the pH of an unknown sample by taking its ratiometric absorbance. A separate correlation was produced for each dye and testing temperature.

Pressure-Correction of Correlation

Changes in the pKa of the indicator dyes due to pressure was determined by preparing solutions of the indicator dye in water at the same concentration as stated previously. The solution was then adjusted to a pH equal to the pKa using dilute HCl or NaOH. Water was used for blank optical determinations. Spectra were taken at five pressures from 0.1 to 400 MPa, blocked by temperature, in triplicate, and random order using the high pressure optical system in Figure 2.1 (a-b). Samples were allowed 5 minutes to equilibrate at pressure before the spectra were taken. The previously developed calibration curves were then used to determine the change in pH with pressure. This value was then used to correct the calibration curve for pressure-induced changes in the dye's pKa at each testing pressure as suggested by Quinlan and Reinhart, (2005). This process was followed for phenol red, bromophenol blue, and bromocresol green.

Pressurized Spectrum Data Analysis

Spectra taken using the high pressure optical vessel showed baseline drift due most likely to the pressurizing fluid. In order to collect accurate absorbance values, all data were baseline-corrected. Modeling the non-absorbing region of the spectrum with a trend line allowed for such correction. Phenol red and bromophenol blue spectra used the region 660 nm to 750 nm, while bromocresol green used 730 nm to 820 nm due to its peak at 615 nm.

Design of Baroresistant Buffer

To confirm that baroresistant buffers were successfully prepared the pressure-corrected calibration curves prepared above were used. For the pH 4 buffer, previously

prepared acetate and n-methylpiperazine buffers were combined to make several solutions of molar fractions 0.1, 0.3, 0.5, 0.7, and 0.9 as well as the pure buffers. Bromophenol blue was added to the samples just before testing to ensure no degradation of the dye occurred during storage. The pH 7 buffer was prepared by combining Tris and tricarballylate buffer along with phenol red dye. Each fraction was tested at 25 °C and five pressures in triplicate and random order. Standard protocol as detailed with the high pressure system description was used when operating the high pressure optical system. The change in pH with pressure was determined through linear regression of calculated pH values at each pressure for each fraction and then graphed against the molar fraction of the buffer mixture to determine the molar fraction that produces little to no change in pH with pressure. Results from the 25 °C experiment were used to narrow the testing of molar fractions down in high temperature experiments.

Results

Indicators Spectra and Solution pH

Solutions of varying pH were prepared using indicator dyes to relate the spectra of the dyes to the pH of the solution. For the acidic buffer, methyl orange was initially used, but was replaced once it was seen that the peak near 500 nm underwent an upwards shift, Figure 2.2. This is due to the delocalization of the charge as the dye switches to its acidic form, Figure 2.3. The protonation of methyl orange occurs on one of the double-bonded nitrogen atoms in the center of the structure and is spread across the entire compound. The two extreme versions of the charge distribution are shown. The spectra of the bromophenol blue solutions are shown in Figure 2.4. As the solution becomes more

basic, the peak at 591 nm increases in height. The inverse is seen for the peak near 440 nm. The peak at 591 nm was chosen for correlation because it had a sharper peak than that at 440 nm and was more sensitive to changes in solution pH. Bromocresol green showed a peak near 614 nm with similar character to bromophenol blue, Figure 2.5. The spectra of phenol red solutions are shown in Figure 2.6. The peak chosen for phenol red calibration can be seen near 559 nm and also increases in height as the solution pH increases.

Figures 2.4, 2.5, and 2.6 allowed identification of isosbestic points for each color indicator, that is, the wavelengths in a spectrum at which two equilibrium species have identical absorptivites (Hoxter, 1979). In this case, it represents an absorbance in the spectrum of a pH indicator dye that does not change due to pH. The peak and isosbestic wavelengths used for each dye are as follows respectively: bromophenol blue (592 nm, 499 nm), bromocresol green (616 nm, 508 nm), and phenol red (559 nm, 480 nm). Figures 2.7, 2.8, and 2.9 represent the ratiometric absorbance against solution pH for bromophenol blue, bromocresol green, and phenol red, respectively.. This relationship mirrors the logistic correlation between the pH of a solution and the dissociation status of a weak acid.

A generalized logistic function was used to model the relationship between ratiometric absorbance and solution pH and is shown in Eq. 3 where L is the lower asymptote, H is the upper asymptote, and Q, B, & v are fitting parameters that help to correct for a lack of symmetry in the data (Richards, 1959). All data fitting was performed in R and the base code is included in the appendix. This model was made for

both indicator dyes at the three standard temperatures used in this set of experiments: 25, 45, and 65 °C. Fitting parameters are listed in Table 2.1. This model provided the lowest residual sum of squares compared to a sigmoid model (Eq. 2.4), both of which had a residual sum of squares of 0.01098. This is nearly ten times more than the residual sum of squares obtained with the Eq. 2.3 which was 0.002194. The improved fit using the generalized logistic equation is due to the increased number of fitting parameters which allowed for a more accurate model of the experimental data. The Bromophenol blue at 25 °C was used for assessment of possible models.

$$Ratiometric\ Absorbance = L + \frac{H-L}{(1+Qe^{-B(pKa-pH)})^{1/v}} \qquad (2.3)$$

$$Y(x) = \frac{1}{1+e^{-x}} \qquad (2.4)$$

In order to make the model pressure-corrected, the change in pKa of the indicator dye due to pressure needed to be determined. The spectra of all indicator dyes were taken at five pressures and three temperatures in order to determine the change for each dye at each temperature. The change in the pH under pressure is approximately equal to the change in pKa as described by Quinlan (2005). Equation 2.3 was used to determine the calculated pH at each pressure tested and linear regression was used to determine the $\Delta pKa/\Delta P$. The pressure-induced change in pKa for phenol red at 25, 45, and 65 °C is shown in Figure 2.10 a-c and the changes in pKa for bromophenol blue at each temperature is shown in Figure 2.11 a-c. This correlation allows for determination of a calculated pH value for the sample. Effects of pressure on the pKa of the indicator dyes

were accounted for as described and compression of solutions was automatically compensated for through use of an isosbestic calibration. The absorbance value at any given wavelength is due to a combination of molar absorptivity at that wavelength, path length, and the concentration. By taking a ratio of the absorbance at two wavelengths, the resulting ratiometric absorbance is actually a ratio of the molar absorptivites at each wavelength and changes with changes in pH.

Baroresistant Buffer Molar Fraction

pH 7 – 25 °C

Quinlan et al. (2005) proposed possible combinations of carboxylic and cationic buffers for preparation of a baroresistant buffer in the biological pH range. Given their small changes in pH with pressure, Tris and tricarballylate buffers were chosen. These two buffers were combined to make a series of solutions with increasing molar fractions of Tris buffer. Quinlan et al (2005) found the molar fraction at 25 °C and pH 7 for baroresistant Tris/tricarballylate was 0.6905. This value was tested and its pressure-induced pH change is shown in Figure 2.12. A linear-regression analysis was performed on the data in Figure 2.12 to obtain a slope value of -0.00015 pH/MPa ± 0.00033. Errors in determination of the slope are reported as standard error. As the buffer mixture was subjected to increased pressure, the calculated pH of the solution showed a shift of nearly 0.06 pH over 400 MPa. This is smaller than their experimental shift of less than 0.1 pH over 400 MPa.

The full range of molar fractions was then tested at 25 °C. Figure 2.13 suggests a theoretical baroresistant fraction of 0.857 and gives a calculated pH shift of 0.0001

pH/MPa for 100 mM Tris buffer. This value is one order of magnitude smaller than those reported by Quinlan & Reinhart (2005) at 0.001 pH/MPa. The increased fraction of Tris calculated in this study would indicate the buffer mixtures tested were slightly more acidic than pH 7, as lower pH values require higher fractions of the cationic buffer for baroresistance. The calculated pH shift with pressure for the calculated baroresistant fraction was 0.04 pH over 400 MPa, Figure 2.14.

As the molar fraction of Tris increases, a deviation from linearity becomes apparent in the graph of calculated pH against pressure. The overall magnitude of the pH shift decreases, but a linear model of the data fails above 200 MPa as illustrated in Figure 2.15. This nonlinear behavior was observed to increase in prominence as the Tris fraction increased. Though the overall magnitude of the pH shift was almost not present when calculated from 0 to 400 MPa, a temporary shift of 0.00034 pH/MPa occurs as pressure approaches 200 MPa and then begins to come back to the original value as pressure approaches 400 MPa.

pH 7 – 45 °C and 65 °C

Fractions of 0.5 to 0.9 Tris buffer were tested at 45 °C and 65 °C for their pH response to pressure (Figures 2.16 and 2.17). A second order polynomial was used to model the relationship and a y-intercept was calculated to be 0.762 for 45 °C and 0.753 for 65 °C. This value represents the molar fraction of Tris buffer in the solution that would produce no change in pH when pressure is applied.

Each calculated baroresistant molar fraction was prepared using the stock buffer solutions and the pH was adjusted to 7 ± 0.05 pH. The baroresistant fraction was then

retested to determine the change in pH with pressure. The results for 45 °C and 65 °C are shown in Figures 2.18 and 2.19. The baroresistant buffer developed for use at 45 °C showed a shift of 0.038 pH over 400 MPa and the buffer for 65 °C showed a change of 0.03 pH over 400 MPa. Both buffers had a basic pH shift with pressure.

pH 4 – 25 °C

A second calibration buffer of pH 4 was attempted following the same experimental outline as that done for the pH 7 buffer. Based on data by Quinlan & Reinhart (2005), 0.1 M acetate and 0.1 M n-methylpiperazine were tested for their baroresistance as well as molar fractions of the two, Figure 2.20. All mixtures of these two buffers resulted in a positive $\Delta pH/\Delta P$, indicating no mixture would result in a baroresistant buffer. In Quinlan & Reinhart's report, acetate was tested at pH 7 where this experiment tested at pH 4 (2005). A solution of 100 mM acetate was prepared at pH 7 and tested using the phenol red correlation, Figure 2.21. Though acetate showed a basic shift at pH 4, results at pH 7 did agree with published data suggesting an acidic shift of -0.0008 pH/MPa at pH 7 (Quinlan and Reinhart, 2005) which is within the 95% confidence interval for the value calculated in this study, which was -0.00075 pH/MPa ± 0.00006.

Additional buffers from Quinlan and Reinhart (2005) were tested at pH 4 to replace the acetate buffer. Succinic and citric acid both had basic shifts at pH 4 under HHP as well as indicated in Figures 2.22 and 2.23. A solution of citrate was also prepared and tested at pH 7. It also showed the same character as acetate, with a basic shift below the pKa and an acidic shift above the pKa. Citrate showed a pH shift of -

0.0017 pH/MPa (Quinlan and Reinhart, 2005) and -0.0013 pH/MPa (Bruins et al., 2007). The calculated pH shift in this study for neutral pH citrate was -0.00217 pH/MPa ± 0.00011.

A series of varying molarity acetate buffers were tested for their ΔpH/ΔP, Figure 2.24. As the molarity of the buffer solution increased, the ΔpH/ΔP decreased showing exponential decay towards a horizontal limit near 0.0003 pH/MPa. This would indicate that the buffer capacity prevents pressure-induced pH changes as well. This was not found by Quinlan for acetic buffer studies at pH 7, where changes of one order of magnitude above and below 0.1 M did not show any change in the ΔpH/ΔP (2005). This would suggest an increasing effect of water and other dissolved impurities in lower concentration buffers, though deionized water was used in both sets of experiments.

pH 4 – 45 °C and 65 °C

Because no suitable baroresistant buffer could be produced for this experiment, a pseudo-calibration buffer was tested instead: 100 mM acetate. This solution was tested with bromophenol blue at 25, 45, and 65 °C as shown in Figures 2.25, 2.26, and 2.27, respectively. They all showed good correlation and linear response with an R^2 of at least 0.85.

Discussion

The use of isosbestic calibration is commonly used in ambient pressure spectral research and corrects for pressure-induced changes in effective concentration and variation of dye concentration between samples (Stippl et al., 2004). However, a more accurate method of baseline correction for high pressure spectra must be developed to

ensure that proper baselining occurs. Upwards drift across the UV-vis region studied was not uniform across the spectral region, nor was a pattern seen as pressure increased, Figure 2.28. This indicates that a complex, possibly nonlinear shift of the baseline occurs during pressurization of samples and would be easily fixed with a set-up that involves a dual beam spectrometer and two optical vessels each holding either the sample or blank for real-time baseline correction. It is likely that some deviation of these results from other methods is due to a non-ideal baseline-correction as pH values were calculated only from the spectra.

Results from this experiment are mixed. Use of the isosbestic calibration gave comparable results for acetate, Tris, and citrate buffers in the neutral pH range when using phenol red, but did not agree with reported data for acidic pH shifts (Quinlan and Reinhart, 2005). Experiments were performed under similar conditions and techniques with the differences being buffer studied, dye used, and pH of solution during testing. We assumed that the pH was not the cause of error as negative pH shifts for acetate and citrate have been reported at comparable acidic pH values as those used in these experiments (Bruins et al., 2007; Hayert et al., 1999). It was also assumed the buffer studied was not the source of error as it has been reported that the pH shift of acidic weak acids is negative with pressure (Nueman Jr. et al., 2010).

Tris buffer had a pH shift due to pressure of 0.06 pH/100 MPa that was smaller than other more pressure sensitive buffers such as citrate (0.15 pH/100 MPa) with both values approximated from graphs of behavior up to 1,000 MPa (Bruins et al., 2007). These graphs of pH vs. pressure were non-linear for most buffers studied beyond 300

MPa. This non-linear shift is likely due to the change in bonds affected by pressure as the pressure is increased (Samaranayake and Sastry, 2010). Above 300 MPa, hydrogen bonds are disrupted and the ionic strength and electric permittivity of the solute become dominant players when calculating theoretical pH shifts.

Bromophenol blue indicator dye displays a color shift from yellow to blue as the pH increases above the pKa near 4. It does not show any change in structure other than the protonation of an anionic oxygen on a dibromobenzene of the complex molecule. The deprotonation of phenol red and concurrent color shift from yellow to red starts a chain of bond shifts resulting in a double bonded oxygen to an aromatic ring and the formation of an anionic oxygen bound to a sulfur atom. Though the mechanism of color change is slightly different between the two dyes, this is also not likely the source of error.

A method of measuring the sensitivity of an isosbestic calibration was suggested by Hoxter (1979). The equation related the change in absorbance 2 nm above and below the isosbestic point of interest in two solutions of the dye with differing analyte concentrations, Eq. 2.5. Ideally, the sensitivity index (I_s) value should be high. The I_s values for bromophenol blue and phenol red at the chosen calibration points were 106 and 121, respectively. Based on this equation, bromophenol blue is 12% less sensitive to changes in solution pH when compared to phenol red.

$$I_s = \frac{|h_A - h_B| + |d_A - d_B|}{0.02p} \qquad (2.5)$$

Where I_s is the sensitivity index, h is the absorbance 2 nm above the isosbestic point, d is the absorbance 2 nm below the isosbestic point, p is the absorbance at the isosbestic point, and subscripts a and b refer to the two solutions of varying analyte concentration.

After comparing the sensitivity of bromophenol blue and phenol red, it would seem that bromophenol blue may underestimate changes in pH when compared to phenol red. This would mean the magnitude of pH changes calculated would be smaller than the actual pH shift, but that the sign would still be the same. Looking back at Figure 2.16, an estimated 0.06 basic shift in pH is calculated for 100 mM acetate at acidic pH while other published data found a -0.4 shift by 200 MPa (Hayert et al., 1999). It is possible that composition of the buffer may account for the error as acetate is a carboxylic weak acid and in all theories would undergo an acidic pH shift regardless of starting solution pH. The contribution of dissolved gasses and other impurities may influence the overall pH shift and a study into the pH shift with solution purity as a factor would shed light on this issue as calculation of the pH shift of a solution matrix is beyond current theoretical models.

The biggest issue with validating results in high pressure pH studies is the lack of a standard reference for data values. pH shifts for acetate range from -0.02 pH/MPa to -0.08 pH/MPa when considering previous studies (Hayert et al., 1999; Quinlan and Reinhart, 2005). Though agreement on the pH shifts of several buffers under HHP exists

among some reports, there is not a consensus when comparing results of all high pressure pH studies currently published, nor is there a reliable theoretical value for comparison.

Theoretical calculations use reaction volumes that are based on infinite dilutions of the weak acid studied. As pressure increases, the concentration will go up, limiting the ability of the theoretical models to accurately predict pH changes (Min et al., 2011). Within the pressures tested in this study, there is also the assumption of homogenous internal structure of water when in reality, different configurations of hydrogen bonding with polar compounds and ions occur (Stippl et al., 2005). These variations and assumptions could lead to errors in predicted pH measurements when compared to those obtained experimentally.

Stippl et al. (2005) states the three major factors needed for developing a robust theory on the effects of pressure on thermodynamic properties are: (1) volume changes when considering nonpolar and uncharged species, the steric geometry change due to pressure; (2) the electrostriction of solute around ions; and (3) the electric field effect of the ion on surrounding solute molecules and its decreasing effect on further away molecules. Eq. 1.1 by El'Yanov and Hamann shows good agreement with measured shifts in pK for ammonium hydroxide by attempting to account for change in reaction volume with pressure as the relationship is not linear, but does deviate by nearly 20% as compared to measured values by 1200 MPa.

Conclusion

A pair of baroresistant buffers for use as calibration buffers in high pressure pH studies was not developed. Molar fraction mixtures of Tris and tricarballylate were found

to have little change in pH with pressure at 25, 45, and 65 °C when prepared to 0.857, 0.762, and 0.753 Tris molar fraction. However, no baroresistant buffer was found at pH 4 and 100 mM acetate was used as a pseudo-calibration buffer. Though results obtained using the phenol red correlation at or near pH 7 agree with published values, the same methodology when applied to the bromophenol blue correlation at or near pH 4 did not show agreeable results. A more extensive study at pH values between 4 and 7 would shed light on the effect of pH on the accuracy of the methodology used. In order for this experimental design for the development of baroresistant buffers to be more accurate, the effect of pressure on the spectra analyzed must be accounted for and a deeper analysis of the source of pH shifts must be performed.

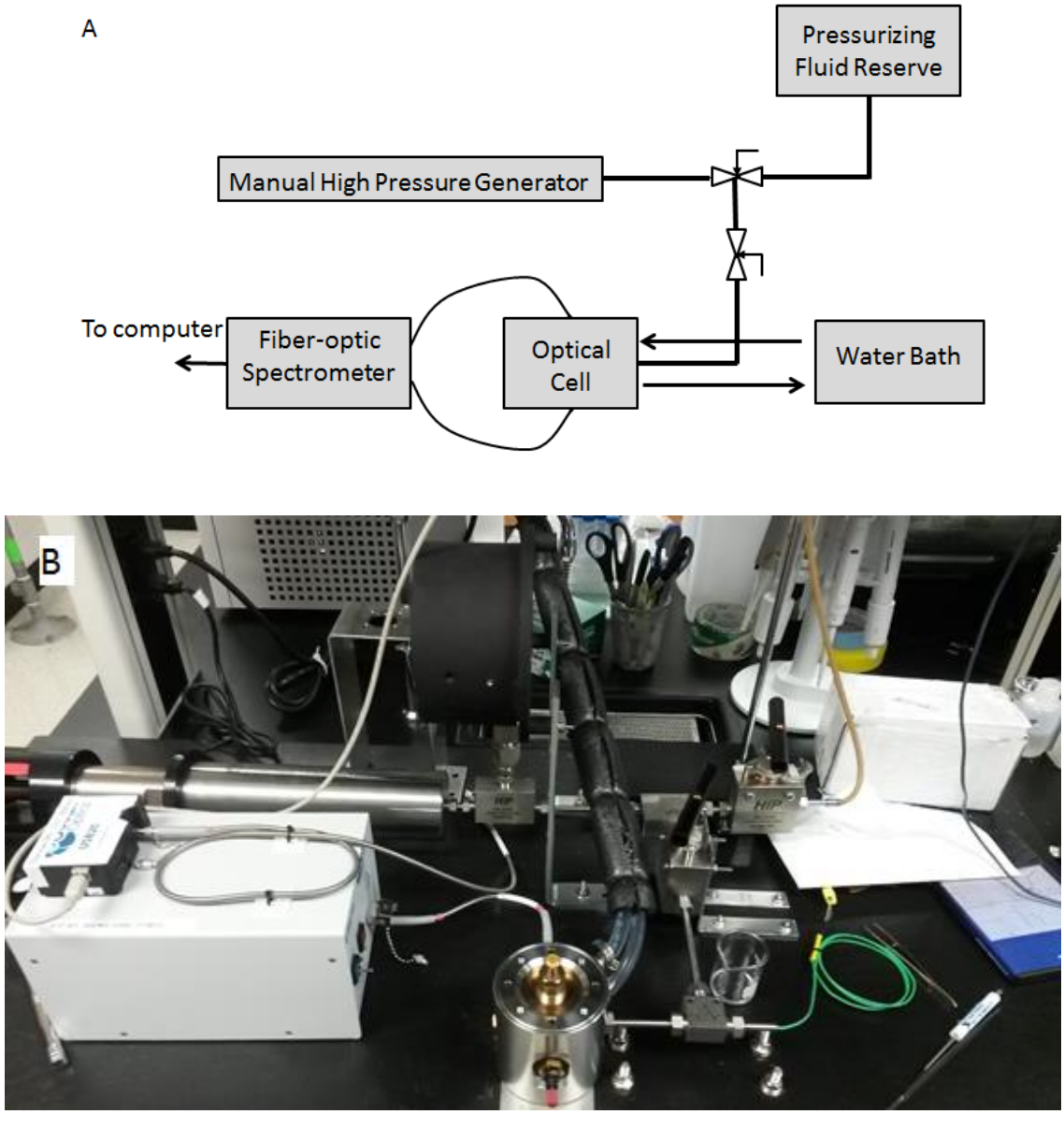

Figure 2.1. High Pressure Optical System. (a) schematic (b) picture

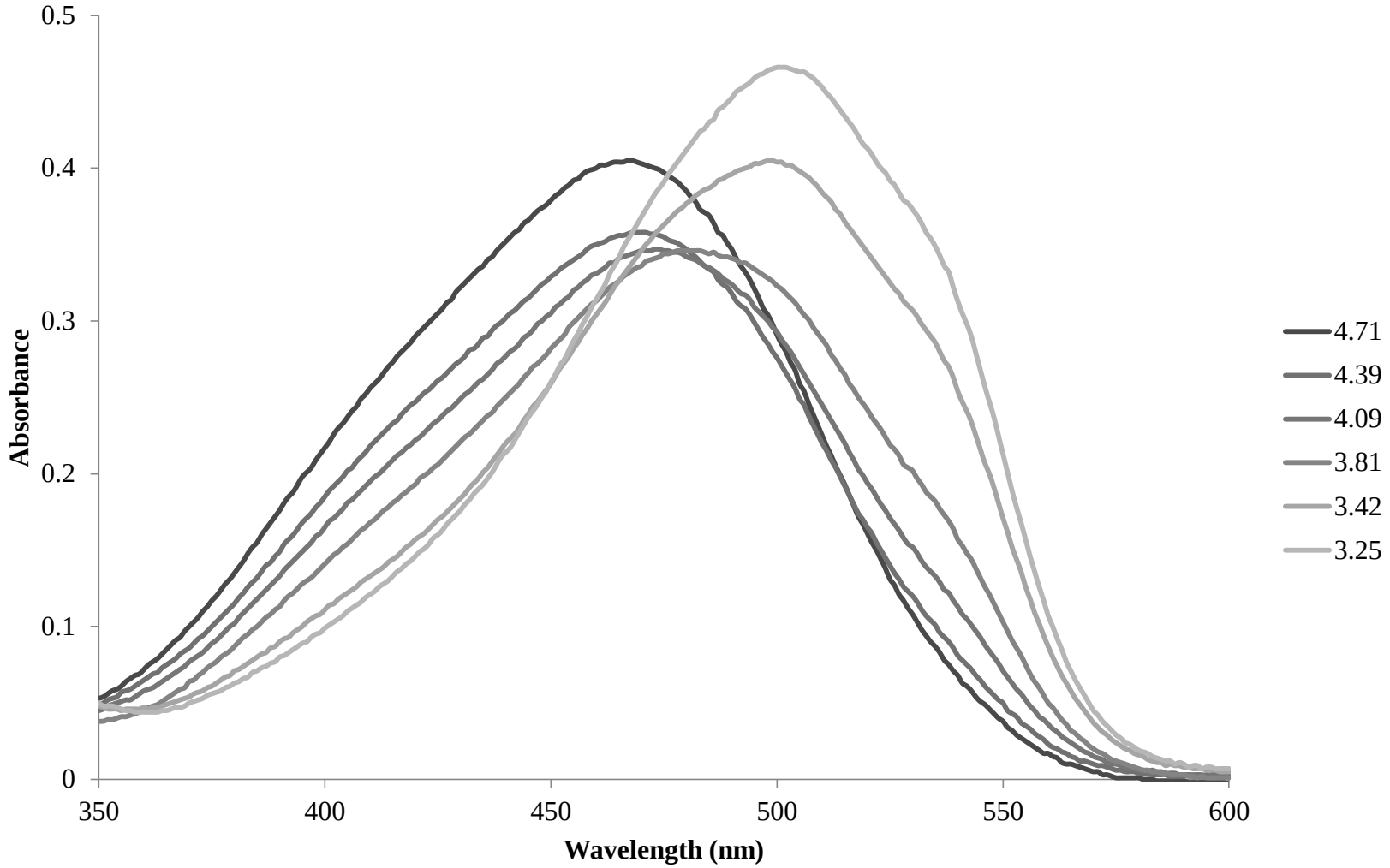

Figure 2.2. Visible Spectra of Methyl Orange at 25 °C at Varying pH Values.

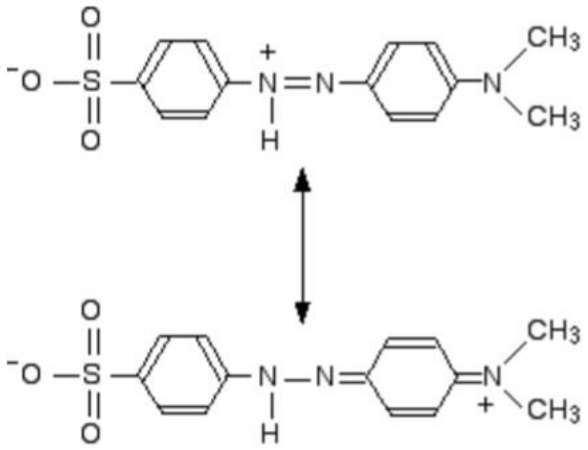

Figure 2.3. Delocalization of Charge in Acidic Form of Methyl Orange.

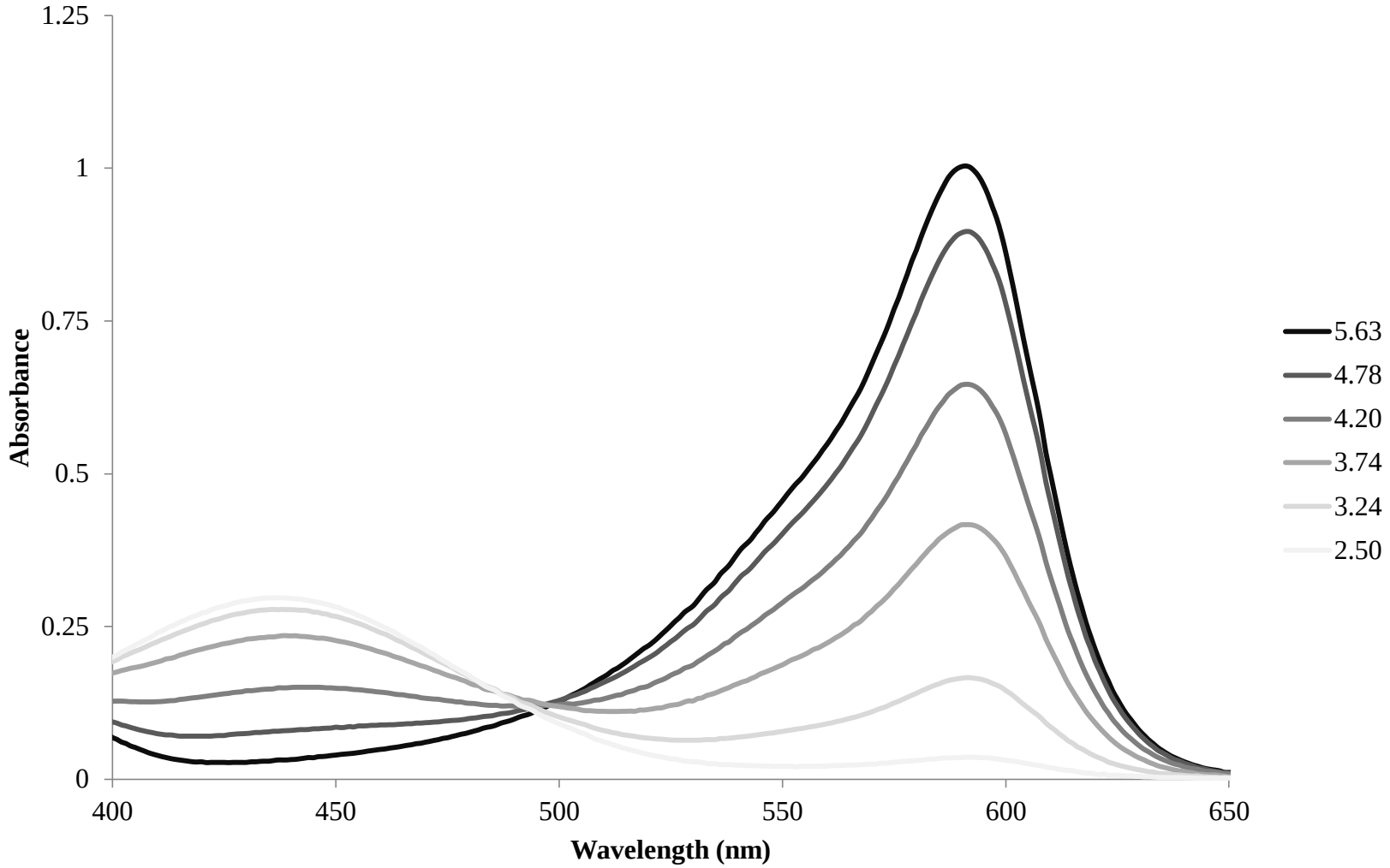

Figure 2.4. Visible Spectra of Bromophenol Blue at 25 °C at Varying pH Values.

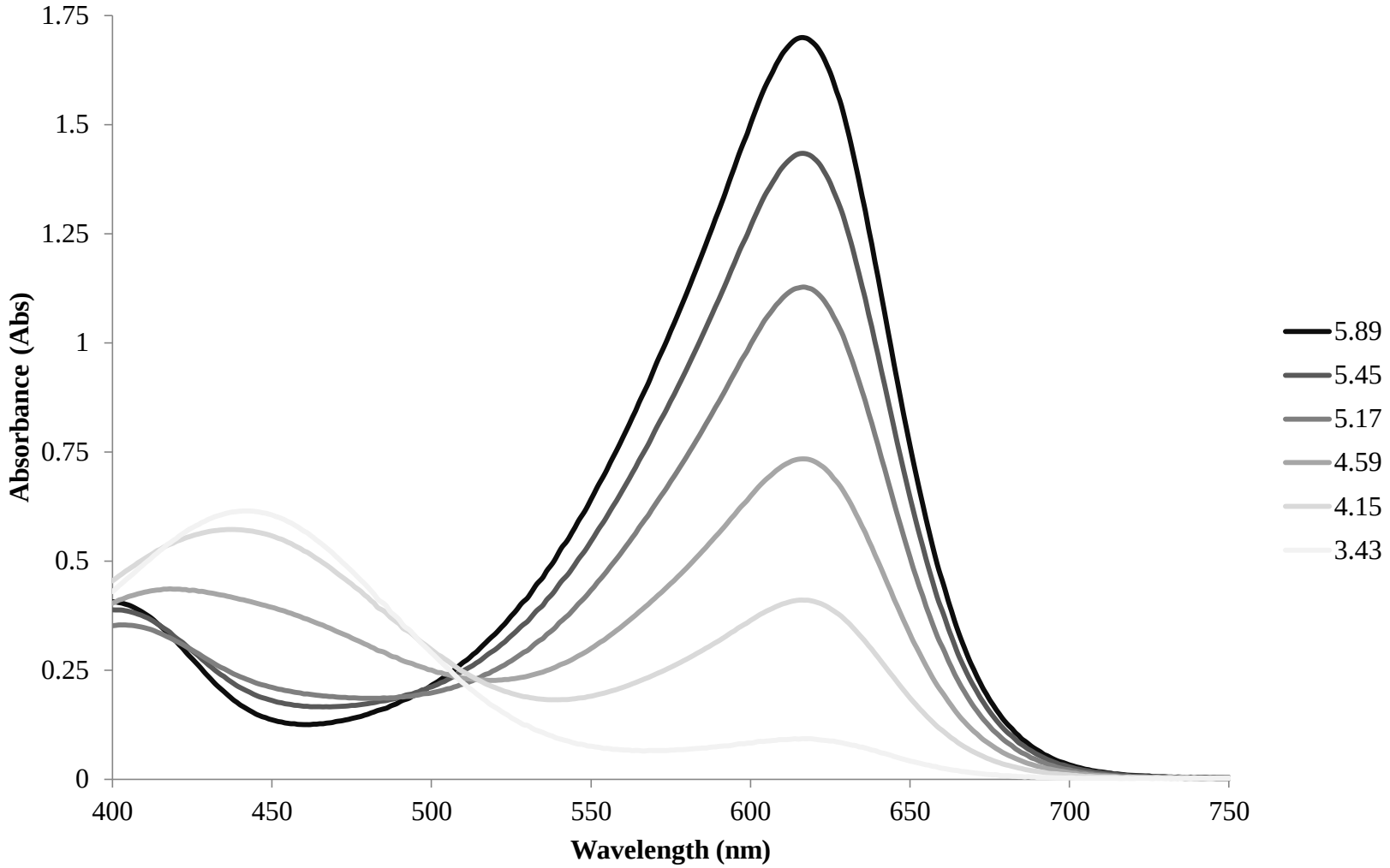

Figure 2.5. Visible Spectra of Bromocresol Green at 25 °C at Varying pH Values.

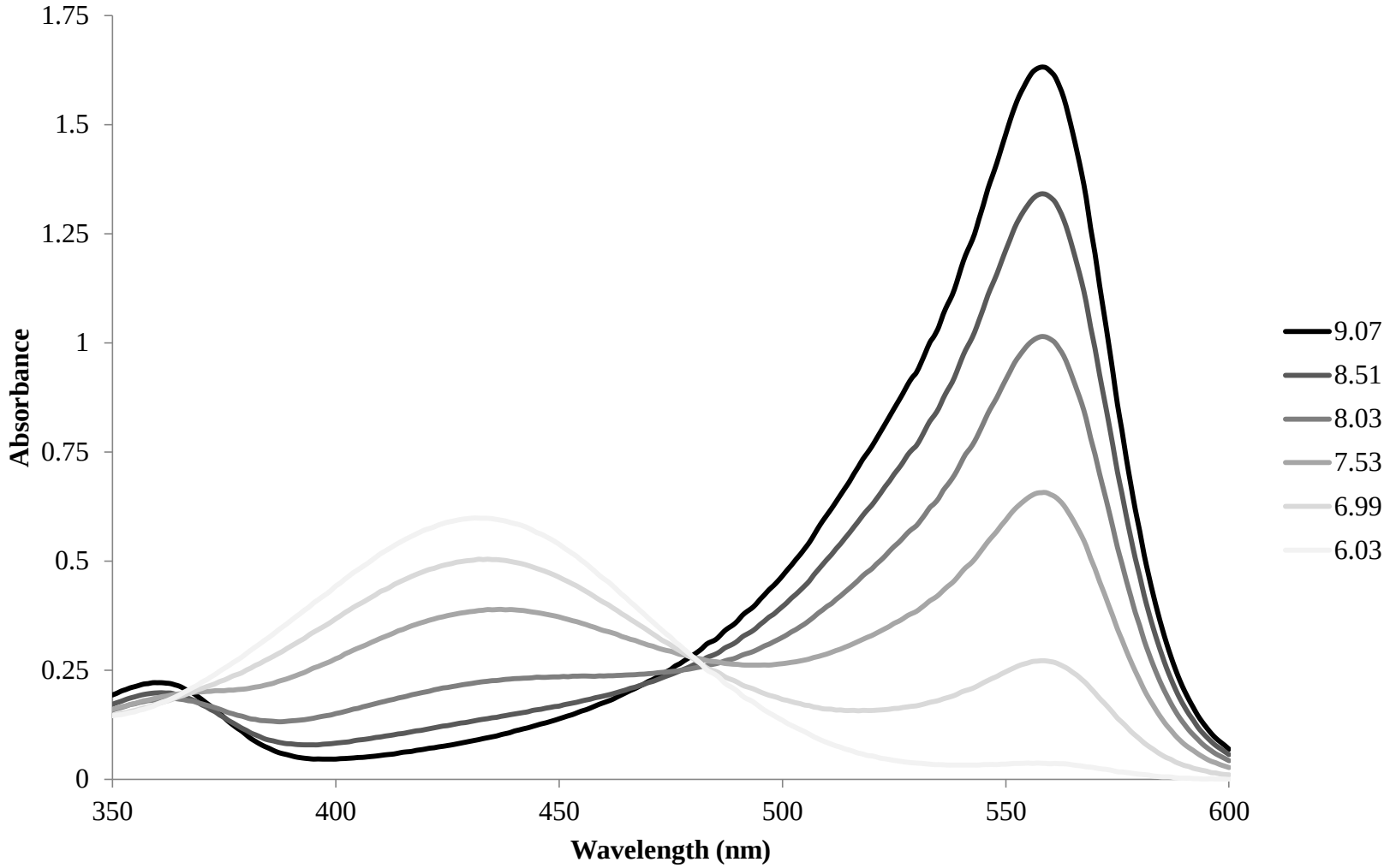

Figure 2.6. Visible Spectra of Phenol Red at 25 °C at Varying pH Values.

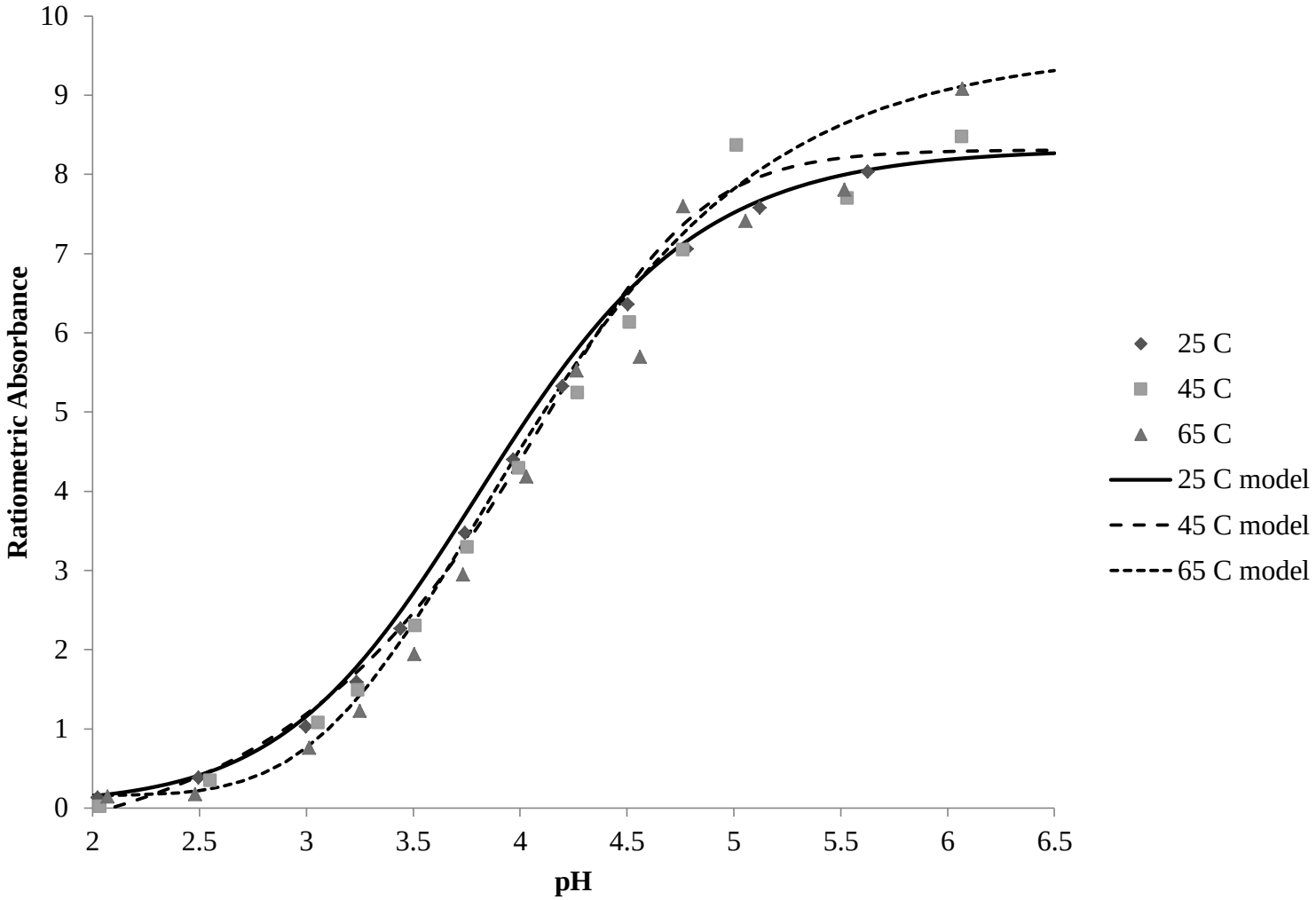

Figure 2.7. Ratiometric Absorbance of Bromophenol Blue vs Solution pH at 25, 45, and 65 °C.

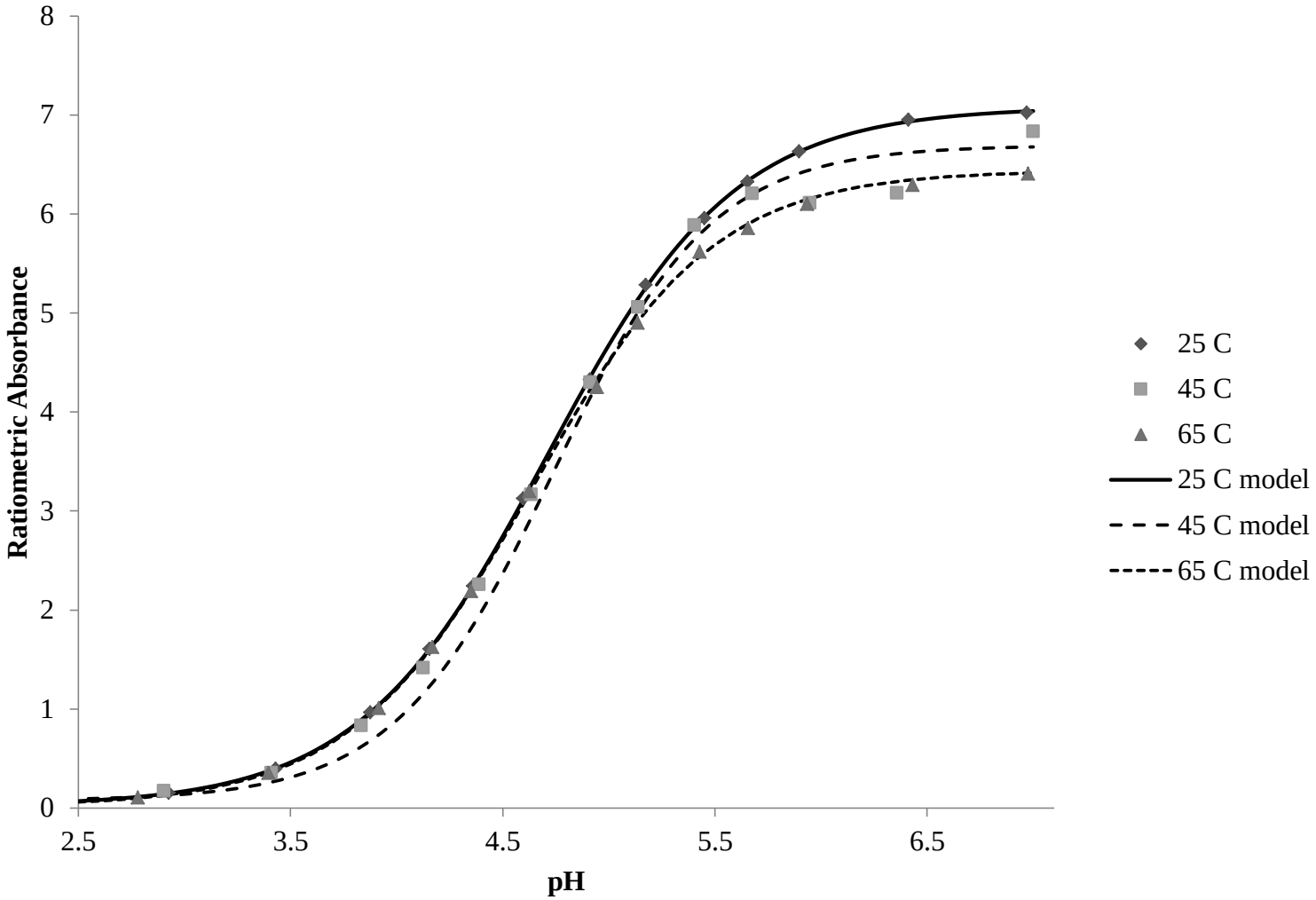

Figure 2.8. Ratiometric Absorbance of Bromocresol Green vs Solution pH at 25, 45, and 65 °C.

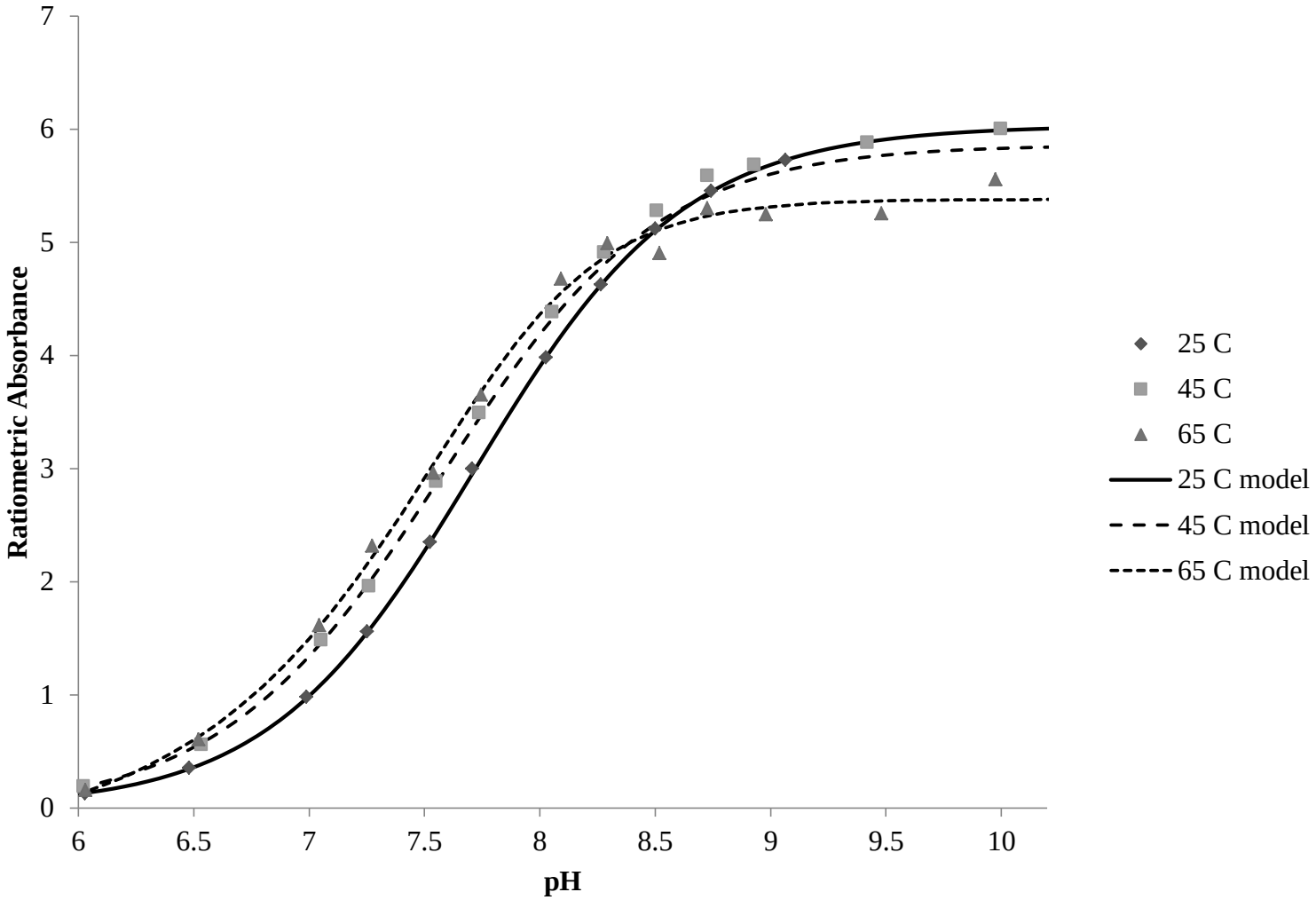

Figure 2.9. Ratiometric Absorbance of Phenol Red vs Solution pH at 25, 45, and 65 °C.

Table 2.1. Fitting Parameters and ΔpKa/ΔP for Indicator Dyes.

Parameter	Phenol Red			Bromophenol Blue			Bromocresol Green		
	25 °C	45 °C	65 °C	25 °C	45 °C	65 °C	25 °C	45 °C	65 °C
L	0.01019	-0.0530	-0.3912	0.04138	-0.7732	0.15901	0.02021	0.07567	0.01532
H	6.03144	5.8610	5.3799	8.32104	8.3094	9.25743	7.07981	6.54148	6.40804
Q	0.49479	0.4331	0.5501	0.53456	6.2611	0.04606	0.65587	0.65547	0.55883
B	-2.17516	-2.1689	-3.0559	-1.86089	-3.2790	-1.32873	-2.25996	-2.68726	-2.36045
v	0.92966	1.0979	2.2855	0.70139	3.2132	0.05426	1.01173	1.16633	1.02820
Residual sum-of-squares	0.00157	0.00558	0.1379	0.00219	0.8482	1.332	0.00231	0.2408	0.01236
ΔpKa/ΔP	-0.00143	-0.00086	-0.00063	0.00053	0.00061	0.00031	0.00070	0.001022	0.000737

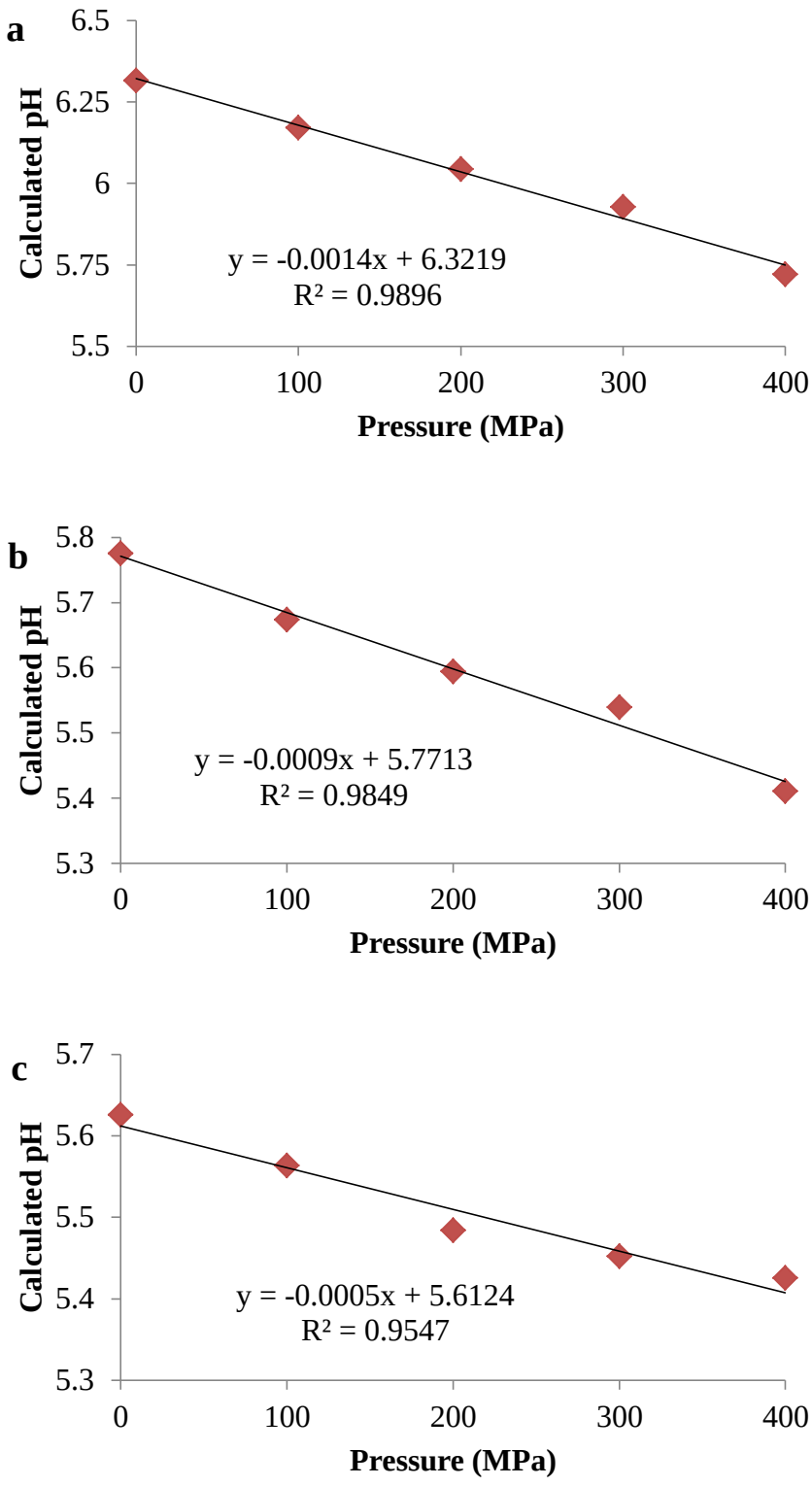

Figure 2.10. Change in pH with Pressure for Phenol Red. (a) 25 °C, (b) 45 °C, (c) 65 °C.

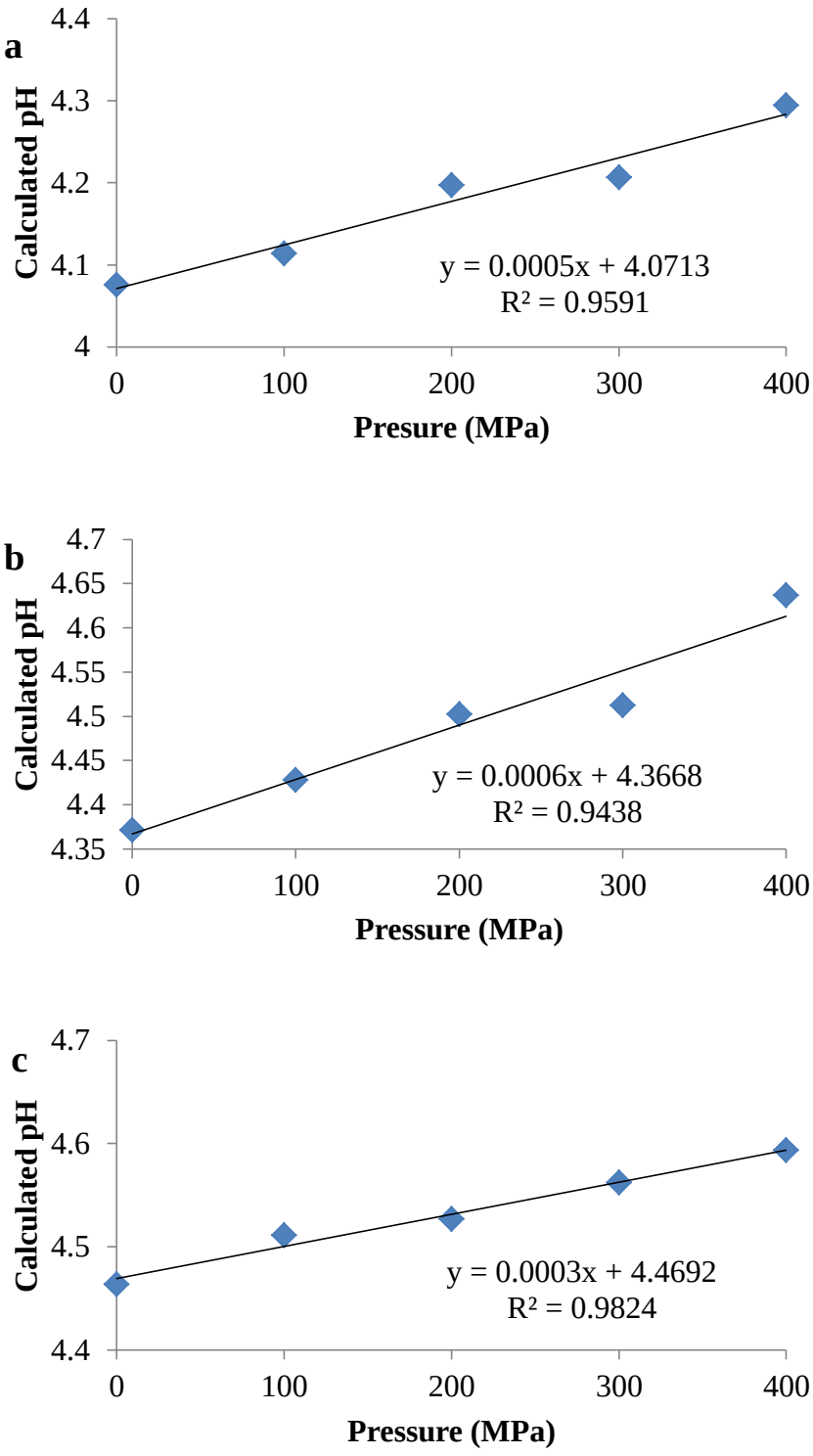

Figure 2.11. Change in pH with Pressure for Bromophenol Blue. (a) 25 °C, (b) 45 °C, (c) 65 °C.

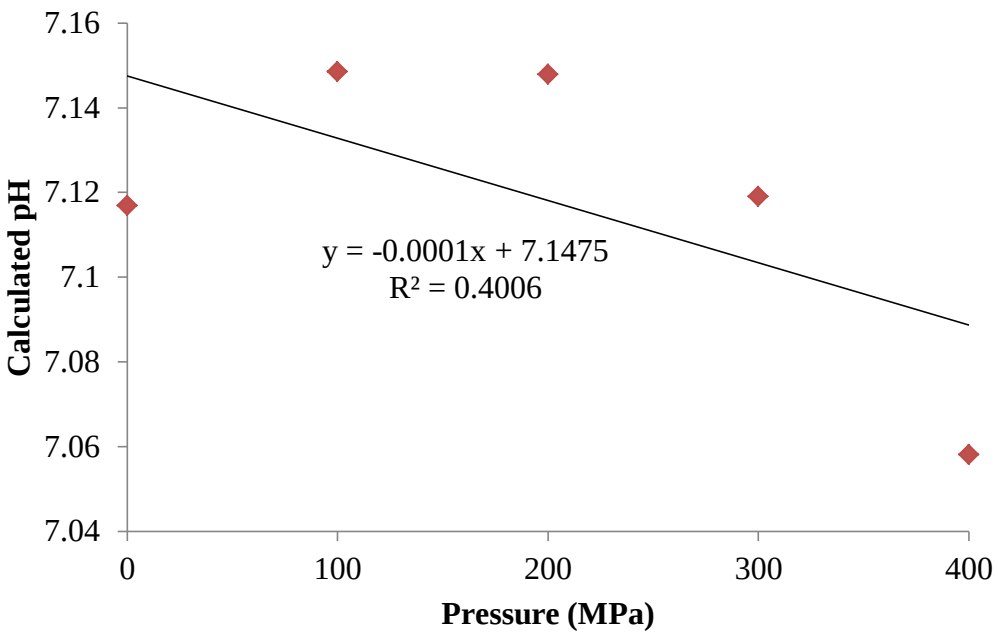

Figure 2.12. Effect of Pressure on the Calculated pH for Tris 0.6905 Molar Fraction at 25 °C.

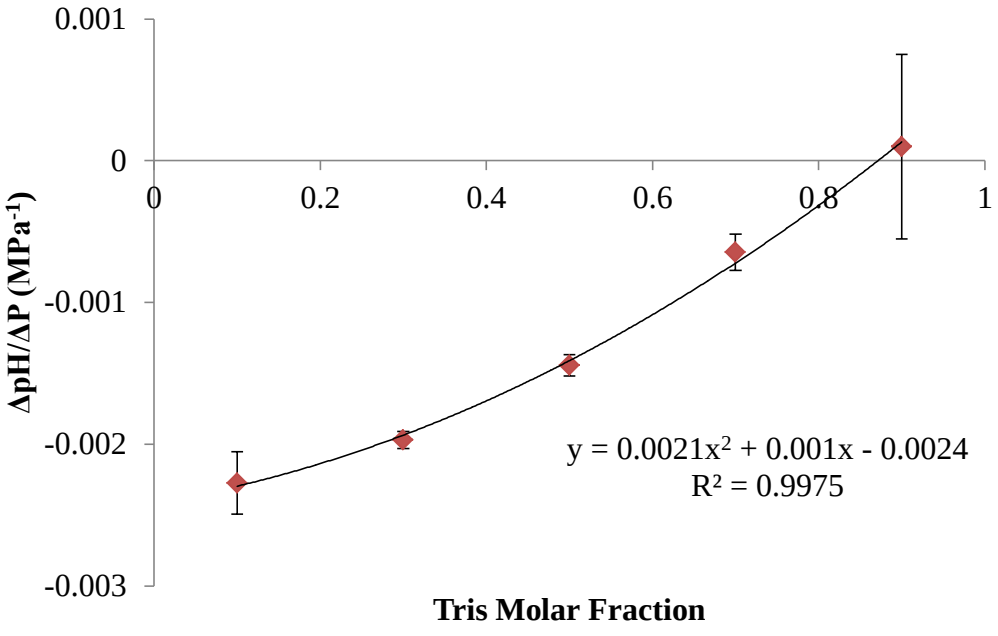

Figure 2.13. Tris/tricarballylate Molar Fraction vs ΔpH/ΔP at 25 °C.

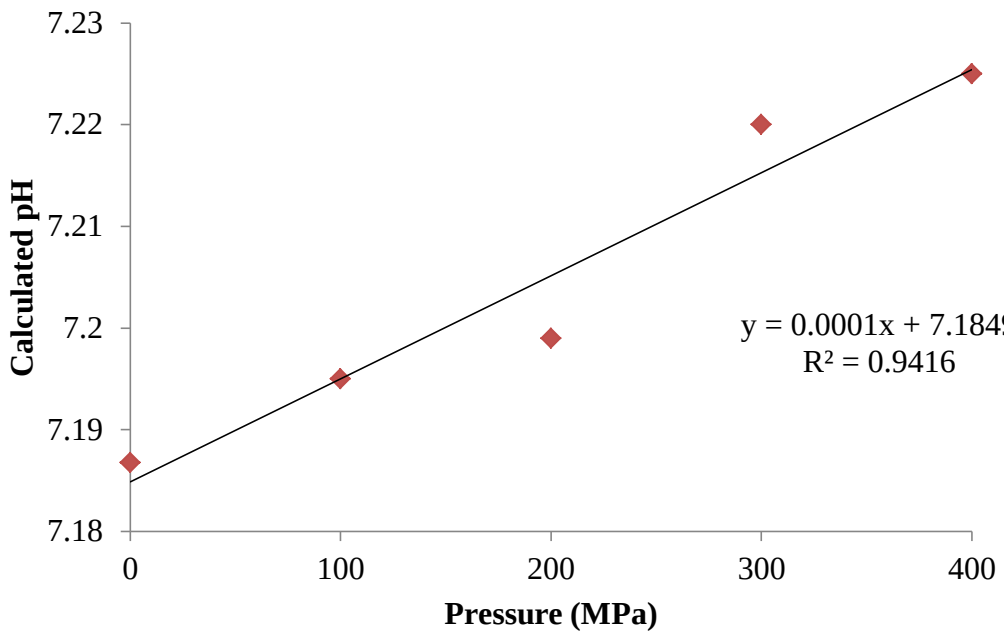

Figure 2.14. Effect of Pressure on the Calculated pH for Tris 0.86 Molar Fraction at 25 °C.

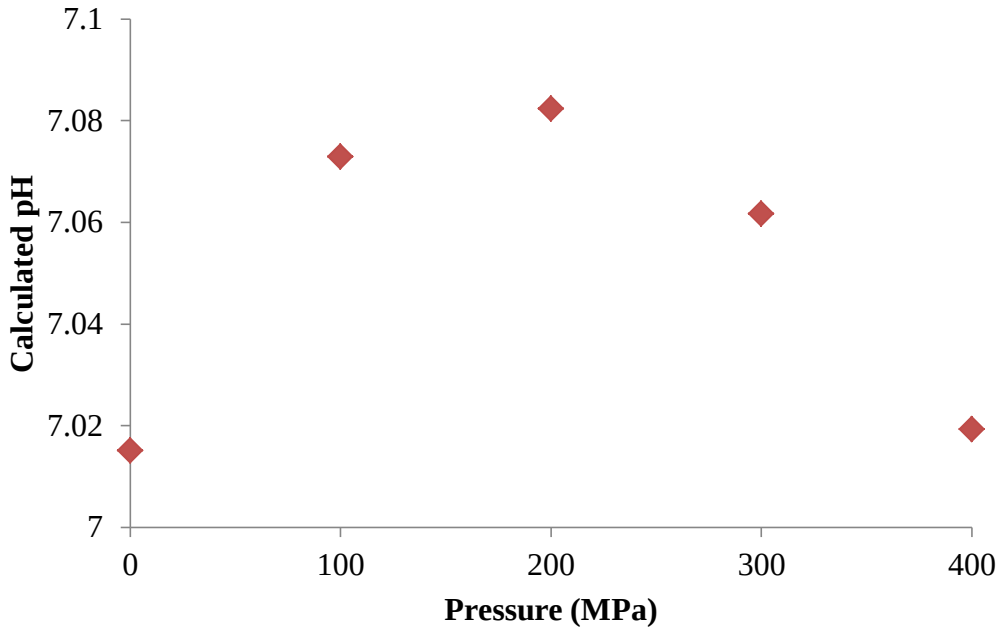

Figure 2.15. Effect of Pressure on the Calculated pH for 100 mM Tris Buffer at 25 °C.

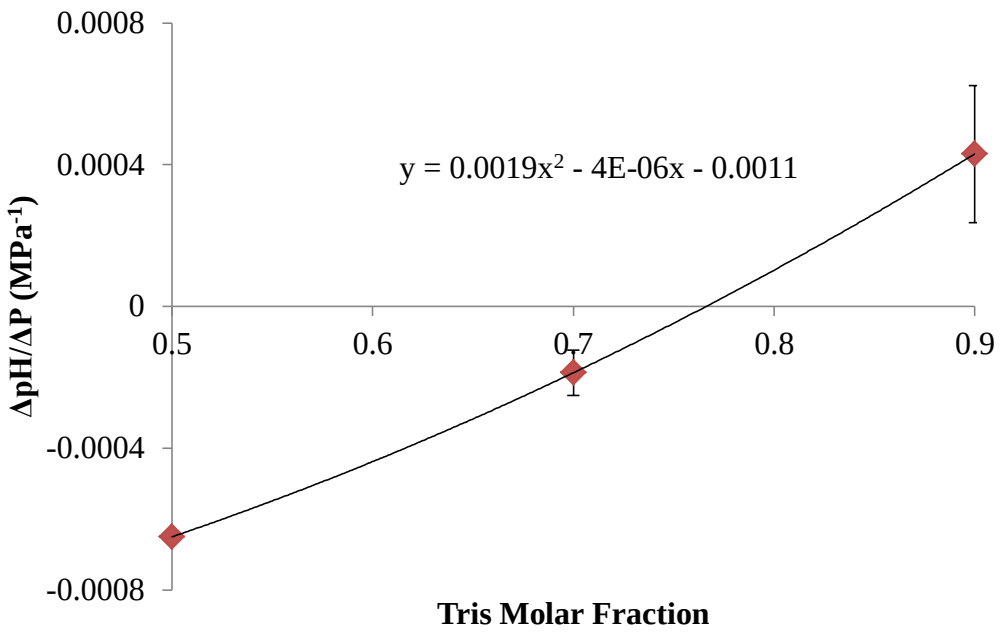

Figure 2.16. Tris/tricarballylate Molar Fraction vs ΔpH/ΔP at 45 °C.

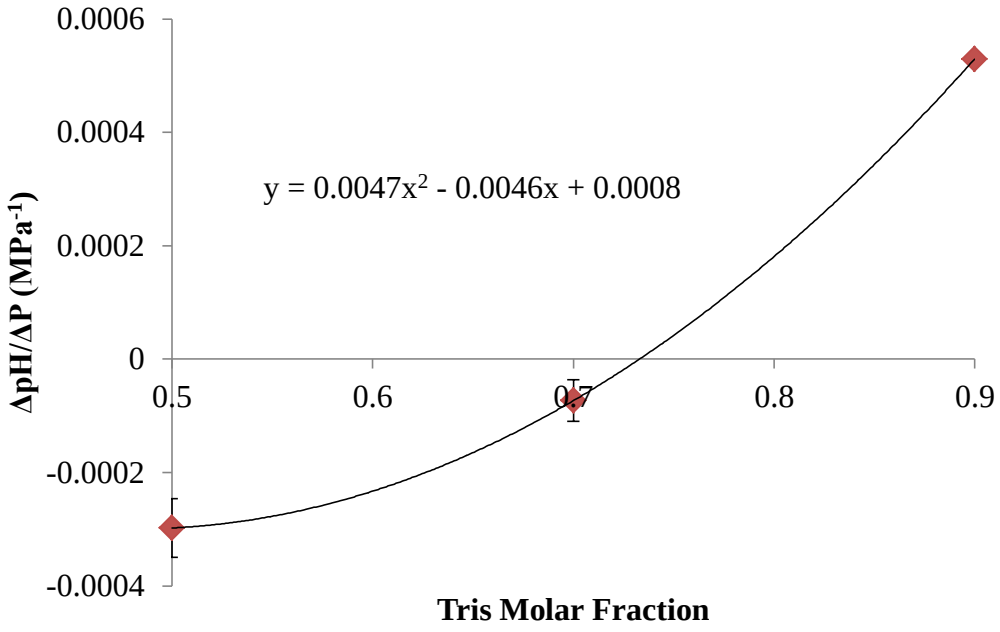

Figure 2.17. Tris/tricarballylate Molar Fraction vs ΔpH/ΔP at 65 °C.

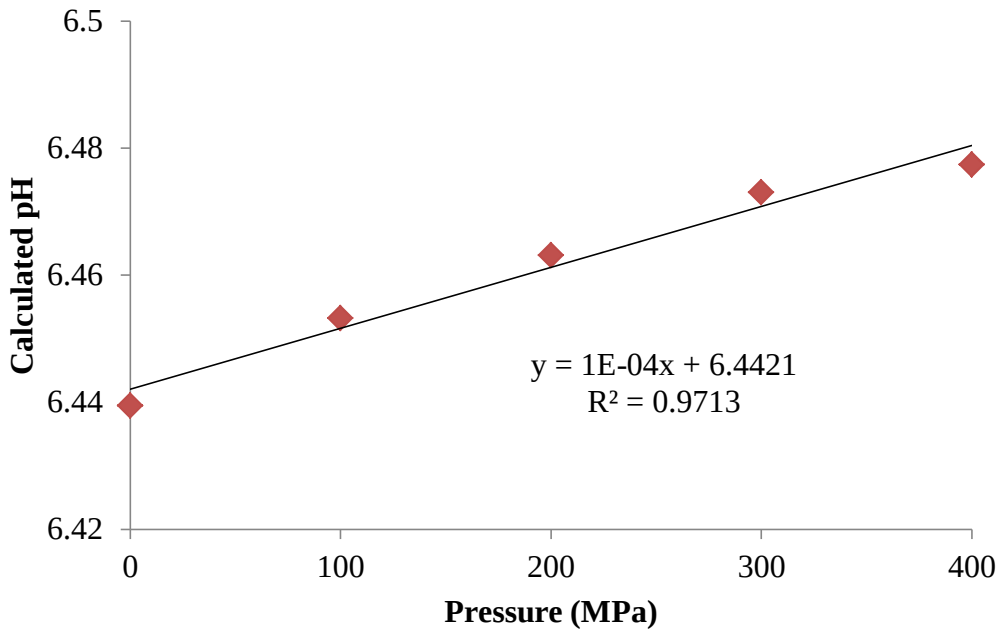

Figure 2.18. Effect of Pressure on the Calculated pH for Tris 0.76 Molar Fraction at 45 °C.

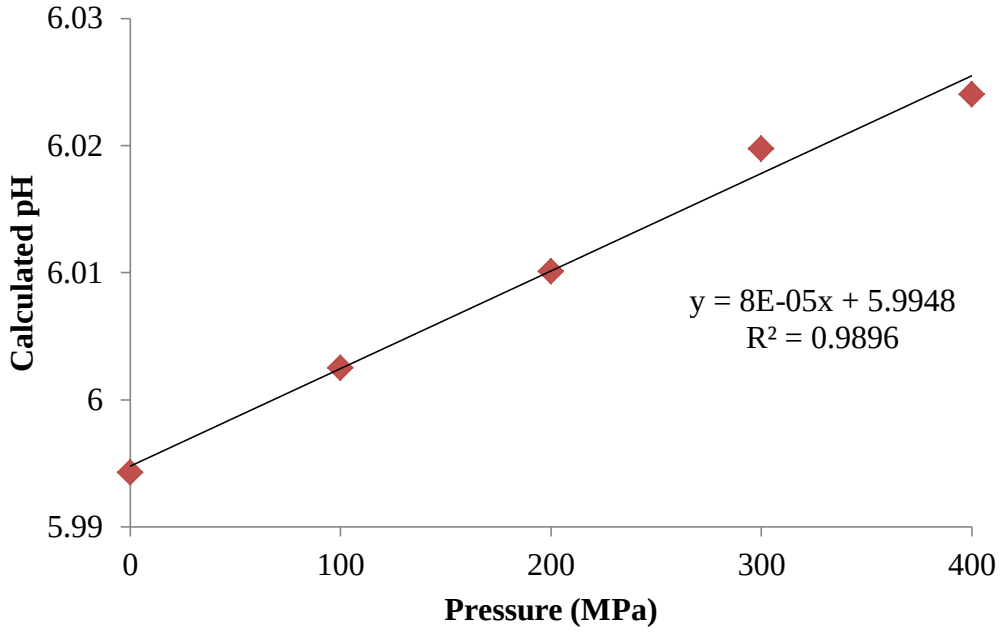

Figure 2.19. Effect of Pressure on the Calculated pH for Tris 0.75 Molar Fraction at 65 °C.

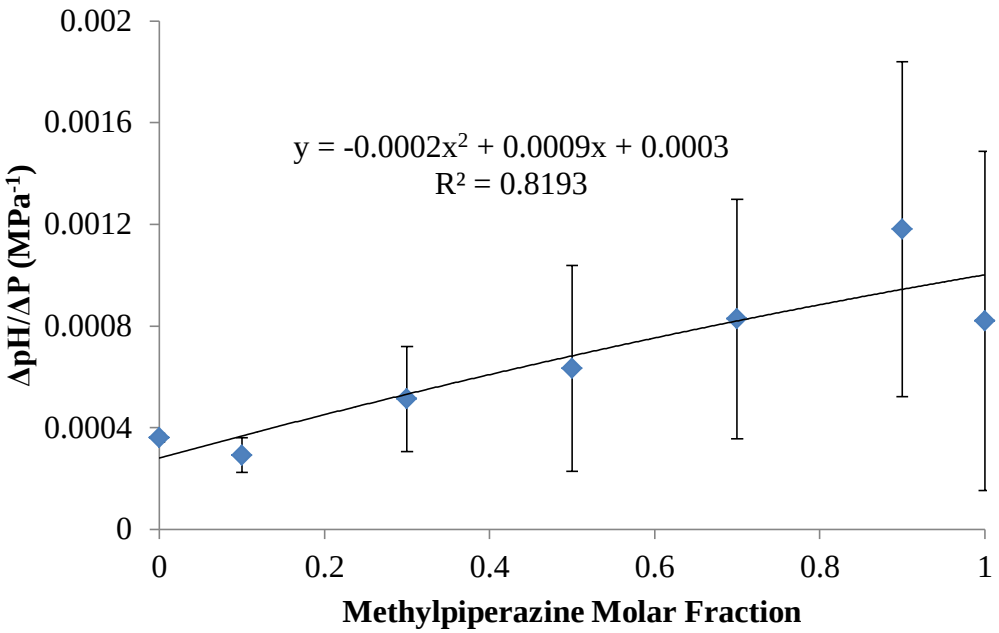

Figure 2.20. Methylpiperazine/Acetate Molar Fraction vs. ΔpH/ΔP at 25 °C.

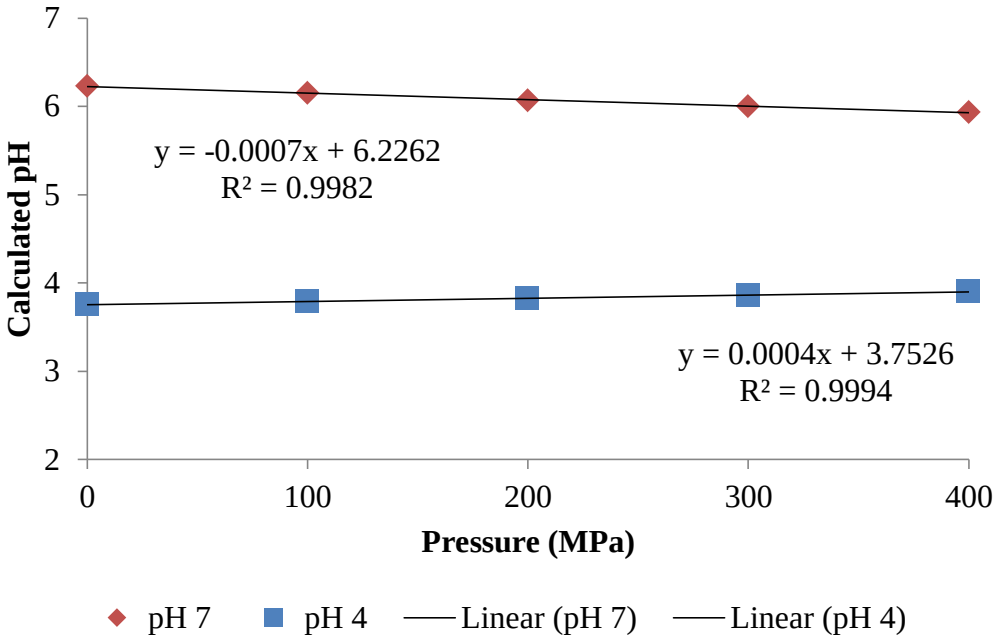

Figure 2.21. Effect of Pressure on the Calculated pH for 100 mM Acetate at Acidic and Neutral pH.

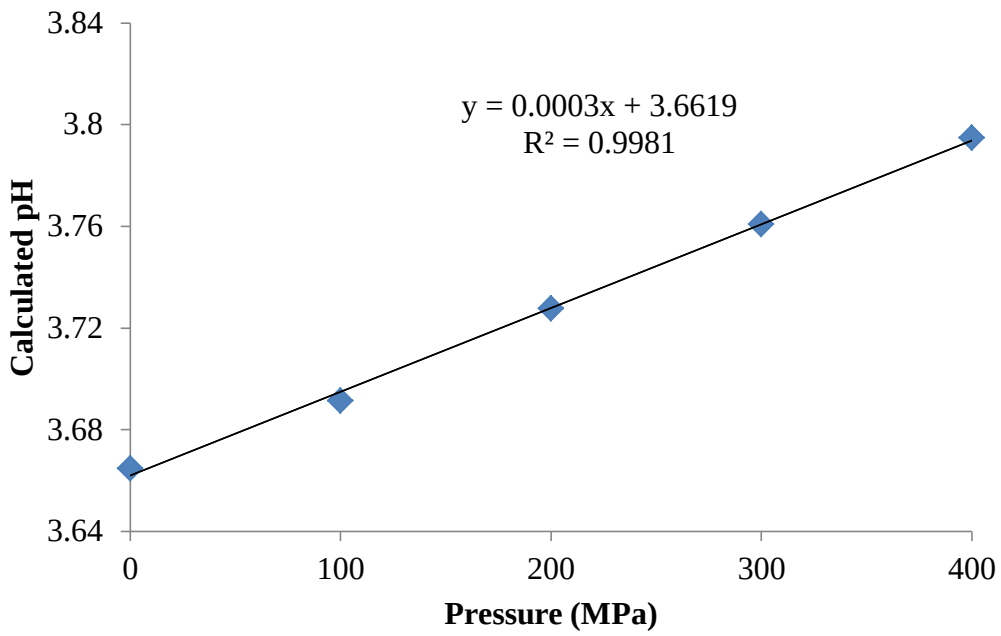

Figure 2.22. Effect of Pressure on the Calculated pH for 100 mM Succinic Acid at 25 °C.

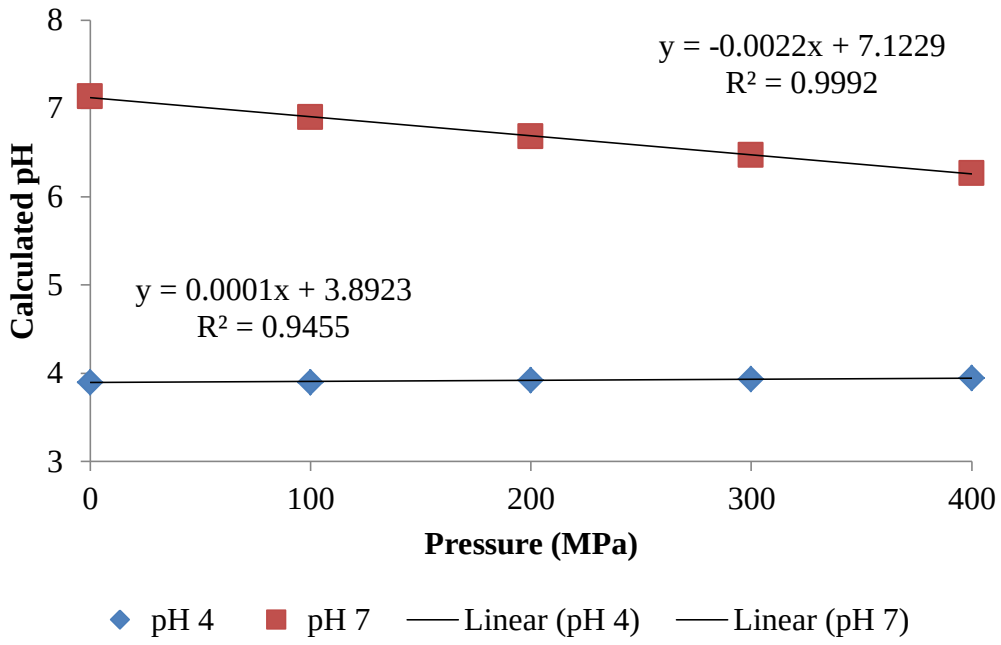

Figure 2.23. Effect of Pressure on the Calculated pH for 100 mM Citrate at Acidic and Neutral pH.

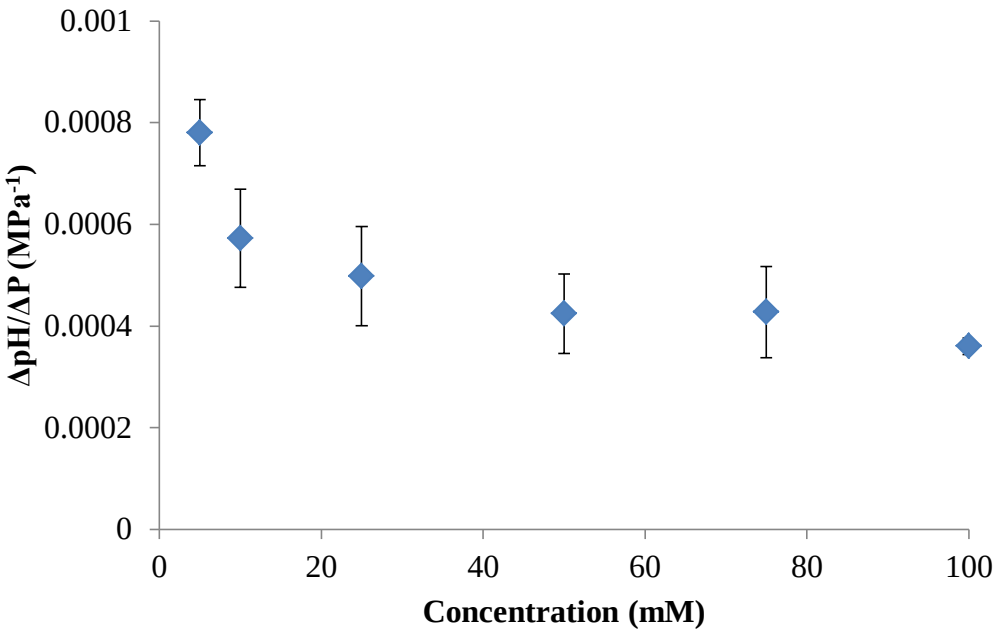

Figure 2.24. Acetate Molarity vs ΔpH/ΔP at 25 °C.

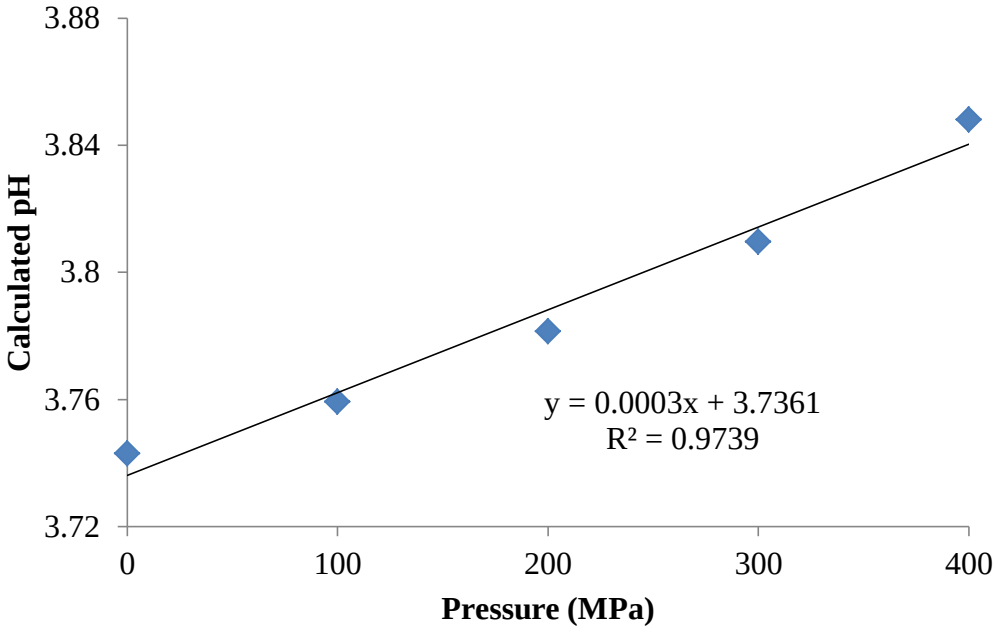

Figure 2.25. Effect of Pressure on the Calculated pH for 100 mM Acetate at 25 °C.

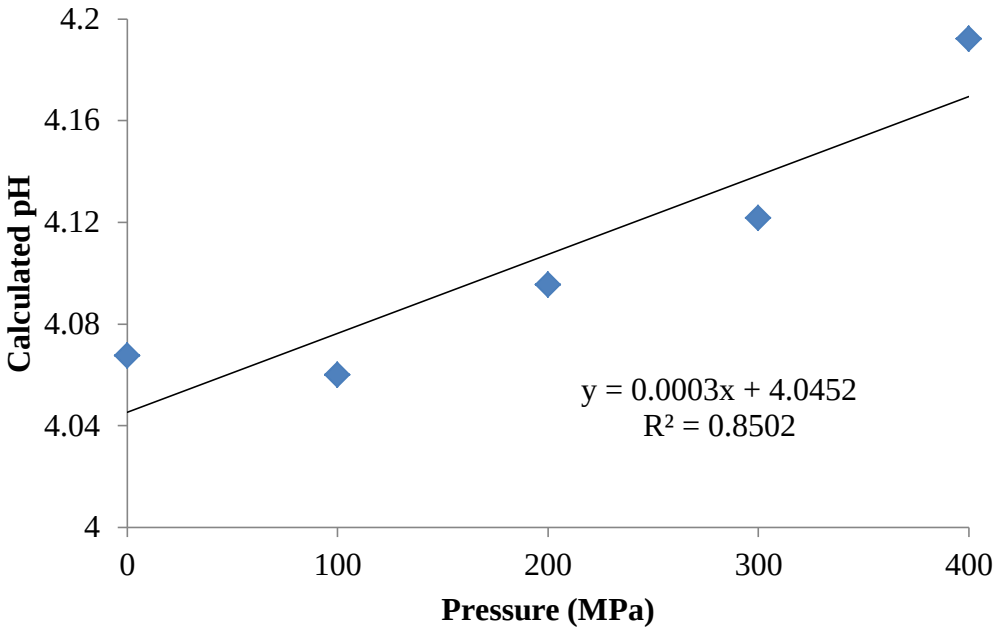

Figure 2.26. Effect of Pressure on the Calculated pH for 100 mM Acetate at 45 °C.

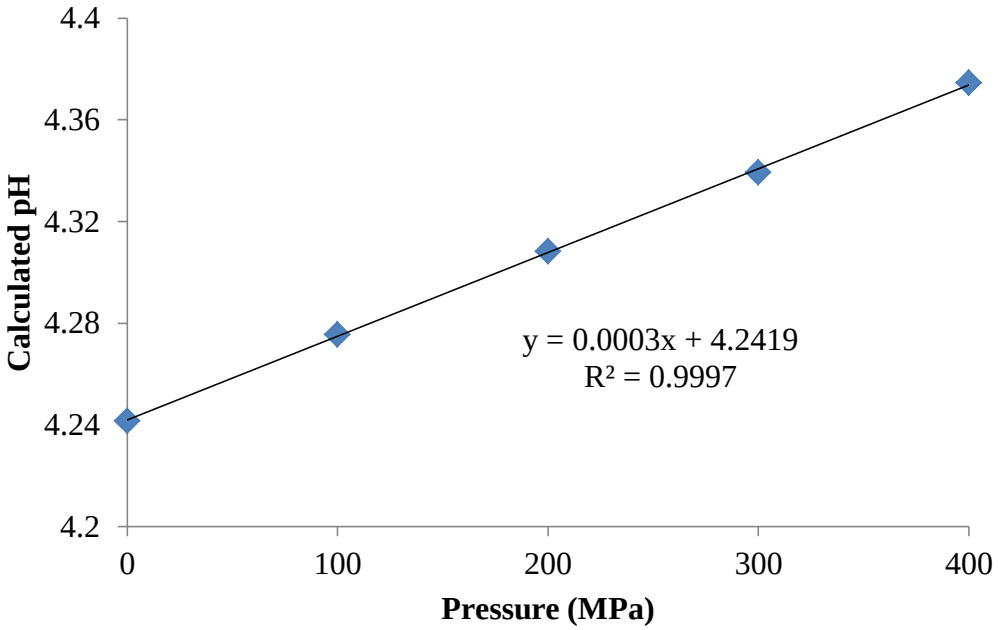

Figure 2.27. Effect of Pressure on the Calculated pH for 100 mM Acetate at 65 °C.

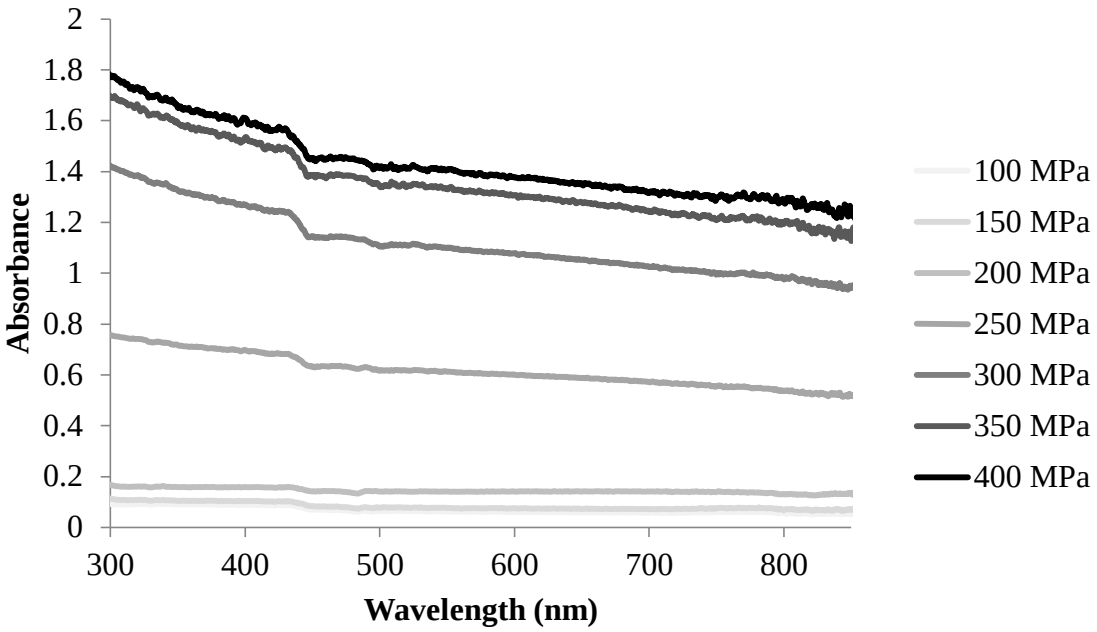

Figure 2.28. UV-vis of Water in Cuvette under Pressure.

References

Bruins, M.E., Matser, A.M., Janssen, A.E.M., Boom, R.M., (2007). Buffer selection for HP treatment of biomaterials and its consequences for enzyme inactivation studies. High Pressure Research 27(1), 101-107.

Hayert, M., Perrier-Cornet, J.-M., Gervais, P., (1999). A simple method for measuring the pH of acid solutions under high pressure. The Journal of Physical Chemistry A 103(12), 1785-1789.

Hoxter, G., (1979). Suggested isosbestic wavelength calibration in clinical analyses. Clinical Chemistry 25(1), 143-146.

Lown, D.A., Thirsk, H.R., Wynne-Jones, L., (1968). Effect of pressure on ionization equilibria in water at 25C. Transactions of the Faraday Society 64, 2073.

Nueman Jr., R.C., Kauzmann, W., Zipp, A., (2010). Pressure dependence of weak acid ionization in aqueous buffers. The Journal of Physical Chemistry A 77(22), 2687-2671.

Quinlan, R.J., Reinhart, G.D., (2005). Baroresistant buffer mixtures for biochemical analyses. Anal Biochem 341(1), 69-76.

Richards, F., (1959). A flexible growth function for empirical use. Journal of experimental Botany 10(2), 290-301.

Stippl, V.M., Delgado, A., Becker, T.M., (2004). Development of a method for the optical in-situ determination of pH value during high-pressure treatment of fluid food. Innovative Food Science & Emerging Technologies 5(3), 285-292.

Stippl, V.M., Delgado, A., Becker, T.M., (2005). Ionization equilibria at high pressure. European Food Research and Technology 221(1-2), 151-156.

Tomlin, B., (2011). Kinetic Behavior of a Pectinase Cocktail at High Hydrostatic Pressure Conditions, *Agricultural Engineering*. University of Florida.

CHAPTER 3

DEVELOPMENT AND TESTING OF A HIGH PRESSURE PH PROBE ASSEMBLY

Introduction

Measurement of pH under high hydrostatic pressure (HHP) presents a series of engineering and theoretical chemistry challenges, the latter of which were covered previously. Furthermore, theoretically calculating the pH shift under pressure of complex food matrices surpasses the abilities of current models which still focus on one compound solutions. A direct measurement of pH under HHP is necessary for accurate assessment of the pH shift for high pressure processed foods. In order to take a pH measurement, a working and reference electrode must be in the test solution and connected to an external signal amplification and conditioning system that can measure the difference in potential, E, across the two electrodes in millivolts. The reference electrode must have a constant equilibrium potential which is used as a reference against which the working electrode's potential in the test solution is measured. A good pH electrode should have a linear response to the concentration of hydrogen ions, generally near -60 mV/pH unit based on the Nernst equation at 25°C for a glass pH electrode.

This response is based on a hydrogen ion-exchange between the solution and the working electrode as the concentration reaches equilibrium. The concentration gradient is offset by an opposing electric gradient which balances the movement of charge from the

solution to the working electrode. The potential is measured against the reference electrode potential and is converted to a pH value using typically a two or three point calibration curve that relates mV to pH using standardized pH buffers at pH 4.01, 7, and 10.01.

Typical pH measuring systems use a glass electrode which combines the working electrode (WE) and reference electrode (RE) in one housing unit. Though extensively studied and universally accepted for having good sensitivity and precision for pH measurements at ambient pressure and a range of temperatures, glass electrodes cannot be used for measurements under high pressure. In order to prevent pressurization fluids from mixing with the internal electrolyte solution, the electrode body would need to be sealed. This would inhibit pressure equilibration and the electrode would break under the applied HHP.

Solid state electrodes are an alternative to glass electrodes as the potential of some solid state electrodes is proportional to pH. Metal-metal oxide electrodes are a type of solid state electrode that is made by depositing a metal oxide film on top of a metal substrate, often times, an inert metal wire. Preparation methods include melt oxidation, plasma deposition, and anodic electrodeposition (Kurzweil, 2009). Iridium oxide (IrOx) electrodes are of particular interest for pH-sensing applications as they have a wide linear response range and little interference from other ions in solution when compared to other pH-sensing metal oxide electrodes, such as PbO_2 whose potential is altered by anions in solution (Kurzweil, 2009). These electrodes are capable of measuring pH in a solution by

forming insoluble hydroxides in the presence of protons, Reaction I. The potential change in IrOx from pH 0 to pH 14 is 825 mV, similar in value to other VIIIb group metals.

Reaction I

$$Ir_2O_3 + 3H_2O + 6e^- \leftrightarrow 2Ir + 6OH^-$$

The objective of this chapter is to design a pH sensing device that functions under high pressure and to calibrate it using the baroresistant buffers developed at pH 4 and 7. This will allow for the determination of pH shifts of food products due to high pressure processing and aid in accurate determination of microbial inactivation rates of pressure-pasteurized products.

Materials and Methods

High Pressure Electrochemical System

Electrochemical measurements at HHP were made using the equipment shown in Figure 3.1 a-b. The high pressure system consisted of a manual high pressure generator from High Pressure Equipment Company (Erie, PA, USA) model #31-5.75-75. Two high pressure needle valves model #A12513 controlled the flow of oil, the pressurizing medium, throughout the system. A pressure gauge from Astra Products (Ivyland, PA, USA) was attached to the system using a connector from High Pressure Equipment Company model #A12381. This allowed for online measurement of applied pressure in 5 MPa increments up to 700 MPa. A connector was also used to provide a connection to the electrochemical reactor. A high pressure electrochemical reactor model U111 was purchased from Unipress Equipment (Warszawa, Poland). The high pressure generator works by pulling out an internal piston that draws in oil from a reservoir. The valve that

connects the reservoir is then closed. As the piston is pushed back into the generator, the oil is compressed producing an increase in pressure throughout the system. Three pin connectors on the bottom of the lid and insulated wires that pass through the reactor's lid allow for electrochemical measurements to be made under high pressure.

High Hydrostatic Pressure pH Sensing Cell Design Considerations

When developing a high pressure pH measurement system, the major concern is to ensure the design is able to equilibrate applied pressure to inside the system where the test solution is held. This requires the housing to be chemically inert so that it does not interact with the test solution, pressurizing medium, and does not contribute to the pH of the solution. The design also needs to be flexible, or have moving parts which allow for transmission of applied pressure. To function properly, the pH probe design needs to have a space for the reference electrode in its electrolyte solution separated by a frit from the test sample solution. The frit allows ion flow between the reference electrolyte and the test solution without mixing of other components. Finally, the design needs to allow for electric signals from each electrode to be transmitted outside of the high pressure reactor to be collected by a conventional pH meter.

Choice of Electrodes

Working Electrode

Metal oxide electrodes were chosen for the working pH electrode as they show linear pH response from pH 2 to 12, high sensitivity, low temperature dependence, and can withstand a variety of solution types including corrosive and nonaqueous (Kurzweil, 2009). Zirconium oxide was initially chosen as the metal is fairly inexpensive and

showed good promise based on papers published using the ZrO electrode for measuring pH in high temperature and pressure environments (Zhang et al., 2010; Zhang et al., 2008). A set of electrodes were prepared following the protocol outlined by Zhang (2010). High purity zirconium wire from ESPI metals (Ashland, OR, USA) was cleaned by sonicating in acetone at 25°C for 30 min, rinsed with distilled water, and allowed to dry overnight. A tube furnace was preheated to 800 °C while the wire was placed in an alumina crucible and covered with sodium carbonate powder (Alfa Aesar, 98%). The crucible was then added to the furnace and the oven temperature was increased to 890 °C which was maintained for 1.5 h. Time and temperature for the melt-oxidation were chosen from the paper to yield an electrode with a continuous film of ZrO_2 on the wire. The wires were left in the furnace overnight to cool down and the carbonate residue was washed off the wires by sonicating in 0.1 M HCl solution. Once cleaned, the larger wires were cut into 3-cm pieces and were coated with iridium heat shrink tubing from Cobalt Polymers (Cloverdale, CA, USA), allowing for both ends to be exposed. The film coat was scraped off on one end of the wire to serve as the electric connection.

Electrode response was measured every 10 s for 10 min using 100 mM acetic acid buffer at pH 4.75 and a Ag/AgCl pellet reference electrode obtained from Princeton Applied Research in 3 M KCl, Figure 3.2. The response took approximately 10 min to stabilize which contrasts to Zhang et al. (2010) whose electrodes responded rapidly to changes in solution pH indicating possible issues with the melt oxidation. This test was performed after refreshing the reference electrolyte in the reference electrode and allowing it to equilibrate overnight.

Five electrodes made from this batch were randomly selected and their potential against an Ag/AgCl reference electrode was measured in pH calibration buffers at room temperature, Figure 3.3. The electrodes did not show a consistent slope magnitude, sign, or character and some simply did not have any change in potential when the pH of the solution was changed.

It is likely that the melt oxidation of the sodium carbonate with the wires did not produce a ZrOx film capable of sensing changes in pH. The procedures did call for a gold-plated crucible which was unavailable at the time of the experiment. This approach was not pursued further and focus was moved to procuring metal oxide electrodes with proven response to pH.

Review papers covering the use of metal oxide electrodes for pH sensing indicate strong potential for the use of IrOx (Hitchman and Ramanathan, 1988; Kurzweil, 2009; Pan and Seyfried, 2008; Wang et al., 2002). This metal-oxygen complex has produced near ideal and super-Nernstian response to pH depending on method of fabrication (Kurzweil, 2009). Super-Nernstian response was achieved by increasing the film's thickness on the wire, but only up to 76 mV/pH after which additional film deposition did not increase the response (Elsen et al., 2009). Sputtered iridium oxide films were deposited on platinum wires by EIC Biomedical (Norwood, MA, USA), producing 2 cm electrodes with the coating covering 0.5 cm of one end of the wire.

A set of 5 wires was chosen to determine sensitivity and slope while the rest were stored dry at room temperature until needed. The potential of the iridium oxide electrode against 3 M KCl Ag/AgCl reference electrode was measured in triplicate and random

order, Figure 3.4. Strong agreement exists between the electrodes not only in slope, but also absolute value. The sensitivity for all electrodes was -59.43 ± 0.89 mV/pH unit. One of the electrodes was used to compare the potential response to solutions adjusted to selected pH. The response of that electrode is shown in Figure 3.5. The slope was super-Nernstian, as it was above the theoretical value of -59.16 mV/pH. The theoretical value is based on a one-electron reaction, and values obtained above it indicate multi-electron reactions possibly due to hydration of the oxidized film. One study compared the thickness of the film coated to the Nernstian response and found that the slope value will increase with thicker films up to -81mV/pH after which it levels out and minimal returns are observed for increased film thickness (Hitchman and Ramanathan, 1988).

Reference Electrode

Typically, calomel or Ag/AgCl electrodes are used in ambient pressure pH measurements and due to the inexpensive cost of pellet Ag/AgCl electrodes; they were purchased for this study from Princeton Applied Research. Other high pressure electrochemical papers have questioned the constant potential of the Ag/AgCl electrode under pressure, but a quick review of their citations show the first authors considered changes in potential to be minimal and therefore regarded the potential as constant over the pressures used (Cruaiies et al., 1992; Min et al., 2011). The compressibility of solid phases and the electrons present in the metallic phase are considered insignificant up to 1,000 MPa. The aquated ions in the electrolyte enhance hydrogen bonding below 300 MPa as hydrogen bonds are not disrupted yet. However, chloride can be thought of as a structure breaker and does not interact with water below 200 MPa.

Combining the overall reaction volumes for the reference electrode system below 300 MPa gives a small enough value to consider the potential constant (Cruaiies et al., 1992). Above this value, a positive shift in potential is observed as metal and crystalline phases promote reduction. The associated reaction volume shows little pressure dependence up to 1,000 MPa and the reference electrode will experience a change in potential of 10-20 mV over 1,000 MPa. For pressures used in this study, the shift in potential would be merely 5 mV. Given the magnitude of the shift when compared to the potential measured by the working electrode, it can be assumed that the reference potential remains constant.

First Prototype

Design

The first prototype is shown in Figure 3.6 a-c. A 6 cm portion of 7/16" OD Teflon water tubing was cleaned and served as the body of the cell. At either end of the cell, 1 cm of 3/8" D Teflon rod from USplastics.com served as end caps. Holes of sufficiently small diameter to only fit the wire of the electrode were drilled into the Teflon plugs. Wire gauge drill bits from widgetsupply.com ranged from 1/71" to 1/69" for the various sizes of wires used during testing of design. A 0.5-cm piece of Teflon rod held a frit in the middle of the cell which would separate both sides and only allow ionic contact between the two half cells. For both the end caps and the frit holder, longer pieces of Teflon were drilled down the center with an appropriately sized bit and sections at both ends of the rod were cut off to remove portions of the drilled hole that were wider in diameter due to entrance and exit of the drill bit. The hole for the frit was drilled to have a

diameter slightly smaller than that of the frit. Once a suitable piece of Teflon was produced, the frit was place on top of the hole and a ruler was used to place even pressure across the top of the frit. This pushed the frit straight down into the holder and had a tight fit.

Testing

This design allowed for use as a pH electrode and as an electrochemical cell as the reference electrode was in a separate compartment from the working and counter electrodes, so testing of the cell design at ambient pressure could be performed using cyclic voltammetry. A cell cap consisting of two gold wires served as the working and counter electrodes while a pellet Ag/AgCl electrode served as the reference electrode. The frit holder was pushed to the center of the cell before any solution was added. One side was filled with 3M KCl to the point of a meniscus above the end of the Teflon tubing. The reference cap was then pushed into the electrolyte to avoid air bubbles in the solution upon closing. The cell was then turned upside to fill the opposite side with 0.5 N potassium ferricyanide, following the same procedure as above. Upon closing the cell with the working and counter cap, leaking of the potassium ferricyanide into the reference cell occurred through the frit holder. There was also leakage through the holes holding the electrodes on both sides.

Second Prototype

In order to reduce problems associated with leaking between cells, the second prototype combined both electrodes on one side, Figure 3.7. This design had the end caps made out of epoxy which were cured with the electrodes in place. The bottom end cap

would have nothing running through it. This was done to avoid leaking through electrode entries and allow for more direct connections to the electrochemical ports connecting the inside and outside of the high pressure reactor, minimizing the chance of a loose connection during testing due to movement of a wire. The epoxy would be cast near the middle of both electrodes. The reference electrode would be prepared using Vycor frits and paired heat shrink tubing from Gambry with a plunger-type modification to the top of the wire to allow transmission of pressure to the electrolyte.

Though this design was an improvement to prototype 1, attempts to make a moveable cap for the reference electrode were extremely difficult as the same leaking around the wire of the electrode from prototype 1 occurred for prototype 2.

Third Prototype

Design

Prototype 2 was changed so that both electrodes were sealed within the epoxy and were not exposed to the pressurizing medium, Figure 3.8. The overall diameter of the design was also reduced to 3/8" to minimize physical constraint in the high pressure electrochemical reactor (HPER). For the working electrode, this simply meant soldering a pin connector to the non-coated end of the wire. The reference electrode was built by cutting it to approximately 3 cm in length and then soldering a pin connector to the non-electrode end. Cold-weld epoxy JB-brand was applied to form a bead of diameter greater than that of the frit on the wire just below the pin connector. Once fully cured, the electrode could be assembled.

The tubing was shrunk in a two-step process. First, heat was applied to the bottom portion of the heat shrink tubing to hold the Vycor frit in place, both of which were obtained from Gamry Instruments Inc. (Warminster, PA, USA). Then, the tubing was filled with 3M KCl. The pellet electrode was then lowered into the tubing and held so that the epoxy bead was even with the top of the tubing and no air bubbles were present within the tubing. Heat was applied to the rest of the tubing and shrunk around the epoxy bead to form a plug holding the electrolyte in. A coating of liquid electric tape was used to seal the cap and tubing to prevent leakage due to non-uniform bead shape, Figure 3.9.

Castin' Craft Easy Mold silicone putty was used to make molds for the epoxy end caps, Figure 3.10 a-b. Teflon rods of 5/16" OD from onlinemetals.com were used to create molds of same diameter and shape. As with the drilling, longer molds were produced and the ends were cut off to improve uniformity in mold shape and size. This served as the vertical portion of the mold. To mimic the angle and spacing of the pin connectors soldered to the inside of the high pressure electrochemical lid, pins were placed in the connectors and then into a flat portion of putty. This was used as the base portion of the mold and held the electrodes in proper geometry during epoxy addition and curing. Some epoxy leaked between the two pieces, but were cut to maintain a circular shape. Five-Minute epoxy from Devcon Home was added to the mold so that it covered the top of the tubing holding the electrode. Frits were kept wet with electrolyte during curing to avoid build-up of crystals. The end product showed sufficient sealing of the reference electrode and proper geometry of the pins, Figure 3.11 a-b.

Upon inspection of the completed product, some black residue appeared within the electrolyte and appeared to be from the liquid electric tape. The pellets also appeared to have turned slightly yellow when compared to their state prior to processing. This color change is likely due to plating of the potassium onto the pellet due to a high molarity of electrolyte in the electrode and slowly returned back to the original grey-brown after regular use. Similarly designed electrochemical cells using a Ag/AgCl reference electrode used an electrolyte concentration of 0.1 M and therefore optimization of the electrolyte concentration would be suggested as an improvement on this design (Cruaiies et al., 1992). Electrode caps were stored so that the reference electrode was in slightly lower molarity KCl and the working electrodes were immersed in distilled water to ensure electrodes were ready for measurements at the start of experiments. Three electrode caps were prepared, but one showed significant and static yellowing and clouding of electrolyte and was taken apart to recycle electrodes for later use.

Testing

A Denver pH meter Model 215 was used to read the potential of the electrodes at ambient and high pressure by splitting the pH cord into its two components and using alligator clips to attach each electrode to the appropriate wire. Both functional electrode caps were immersed in pH calibration buffers 4.01, 7, and 10.01 from Thermo Scientific and had their potential measured, Figure 3.12. Each cap was tested individually, using the internal reference electrode and an external Ag/AgCl reference electrode, in each buffer in triplicate and random order. Though the absolute potential values measured for each cap differed between reference electrodes, the slope stayed at -40 mV/pH. This showed a

33% decrease in sensitivity after processing the electrodes. Without electron imaging of the working electrode's surface, it is impossible to say whether this decrease is due to damaging the film or if it is due to the cell design.

The design's ability to withstand pressure was also tested by filling the cell with water and closing it with one bottom cap and one electrode cap. The cell was then attached to the inside of the high pressure electrochemical reactor (HPER) lid and potential was read on the Denver pH meter. The cell was subjected to increasing pressure at 50 MPa intervals and checked for an adequate connection between the cell and the lid by measuring potential during pressurization. When an adequate connection was lost between the reactor lid and the cell, measured potential increased to nearly 1,000 mV. The cell and pressurizing liquid were also observed for any water or oil movement following depressurization of the system. At all pressures, a secure electrical connection was maintained and minimal water movement out of the cell was observed.

Cell Calibration

Potential measurements using the electrode cap were made at 25 °C in the pH 7 baroresistant buffer (0.865 Tris molar fraction) and 100 mM acetate at pH 4.0 at 0.1, 100, 200, 300, and 400 MPa through use of the HPER and the Denver pH meter. The electrode cap was inserted into the cell body and filled with solution. Air bubbles were removed by bending and twisting the tubing. The cell was closed by pushing the bottom cap into the solution, again attempting to minimize presence of air bubbles. The cell was then attached to the lid by pushing the pins into the pin connectors until a secure connection was established after which the lid was placed onto the HPER and closed. The pH meter

was attached to the appropriate wires coming out of the HPER lid and the system was pressurized to the set pressure. Potential values were recorded following a five minute period which allowed for stabilization of the reading and equilibrium of the pressure, Figure 3.13.

The cell showed very low precision within measurements at the same pressure with some overlap between the two buffers at 400 MPa. The mean potential measured for each buffer at all pressures did show a larger value for the acidic buffer which was observed for the electrodes prior to processing. The sensitivity of the cell at ambient pressure was further reduced to -33 mV/pH, almost half of the original slope. Approximate slope values at high pressures showed no pattern and were inconsistent throughout the pressure range tested, Figure 3.14. Assessment of the cell design and measurement system at ambient conditions as compared to sensitivity measured with fresh electrodes and after potting in epoxy in shown in Figure 3.15. The electrode sensitivity to pH decreased after being cured in epoxy to -42 mV/pH. A further decrease to -33 mV/pH was observed when making measurements of potential using the completed cell design and in the high pressure reactor. This shows that a voltage drop occurred to the potential measurements coming from the working electrode due to the electrode cap design and the electrochemical reactor lid and the wiring between it and the pH meter. The overall net loss in sensitivity is nearly 50% of the original Nernstian slope response.

Discussion

The final prototype showed promise for use in high pressure pH measurements. The physical stability of the design under pressure held up to the minimum conditions required for the design: to equilibrate internal and external pressure and to have minimal oil/water movement during pressurization, though there is room for improvement. Water was observed to leak out of the design intermittently, indicating either a lack of consistency with cell assembly or incomplete drying of cell prior to immersion. Water in the pressurizing oil decreased when the caps were pushed further into the cell body.

The design of the reference electrode may have led to a drifting potential as there was no design functionality included to transmit pressure to the electrolyte other than through the frit and compression of the tubing. This was observed at ambient pressure as a 2 mV/min drift that went on for well over 10 min. However, ambient pressure measurements showed the reference electrode component did function properly when compared to an external reference electrode. Improvements on this design should primarily focus on the reference electrode. Solid-state options are available which would minimize the physical design requirements, but their potential variation with pressure would need to be known in order to correct for pressure-induced changes (Lorant et al., 2012).

A decrease in the sensitivity of the working electrode occurred as the electrode was altered by soldering and potting in epoxy. The electrodes did show some sensitivity to pH, but were too insensitive and imprecise to be used for analytical measurements under the testing conditions. Initially, the electrodes obtained a slope of -59 mV/pH, but

this value was reduced to -40 mV/pH after being sealed in epoxy. The decrease in potential indicates that a voltage drop was added to the working electrode circuit as the electrode was processed. This is likely due to the epoxy, soldering, or longer wired connections, as these were the only changes to the working electrode before the sensitivity decreased. The iridium oxide film on the electrode may have also been damaged or worn off, but this can only be tested through use of microscopy to observe the film in detail.

Conclusion

The design presented shows promise for in-situ measurement of pH under high hydrostatic pressure, but will require improvements in sensitivity and precision before use in analytical experiments. Improvements should focus on preparing a pressure-resistant reference electrode with either a pressure-independent potential or a well-known dependent potential. The circuit should also be adjusted to minimize voltage drop encountered by the electrode pair to increase measured voltage and improve sensitivity. The effect of pressure on the sensitivity of the working electrode should be investigated by measuring the voltage of the electrode in a baroresistant buffer as pressure is increased. This will help to determine if lack of precision in high pressure measurements was an artifact of the randomized experimental design or if it was due to changes in how the electrode functions under pressure.

In addition, improvements in the sensor's accuracy will depend on improving the calibration method. The baroresistant buffers developed in Chapter 2 show potential for further high pressure electrochemical studies, but the data must be validated first. Due to discrepancies between experimental and published data, a deeper look into alternative indicator dyes and more accurate baseline correction methods must be performed to find the source of error.

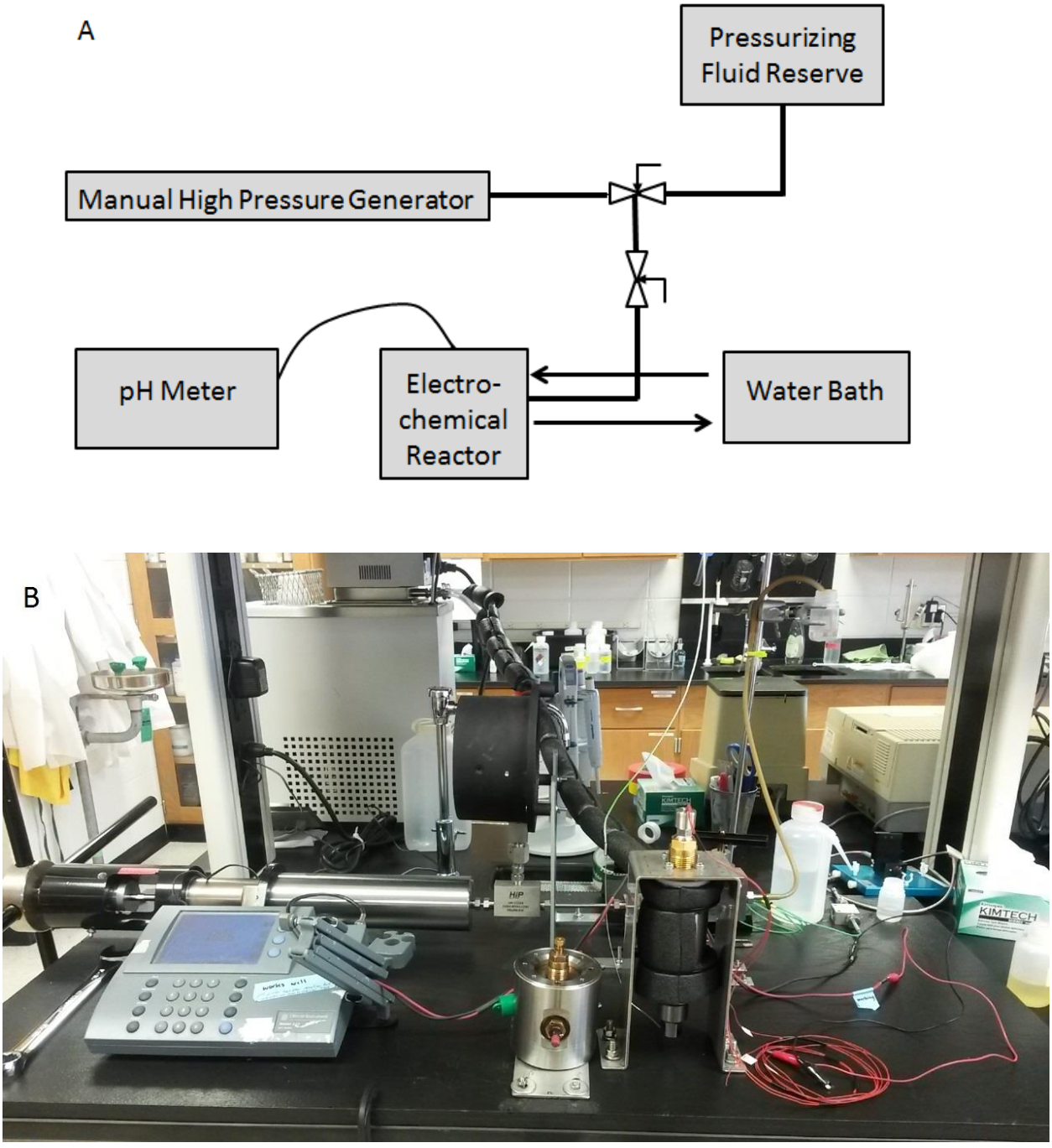

Figure 3.1. High pressure electrochemical system. (a) schematic (b) picture

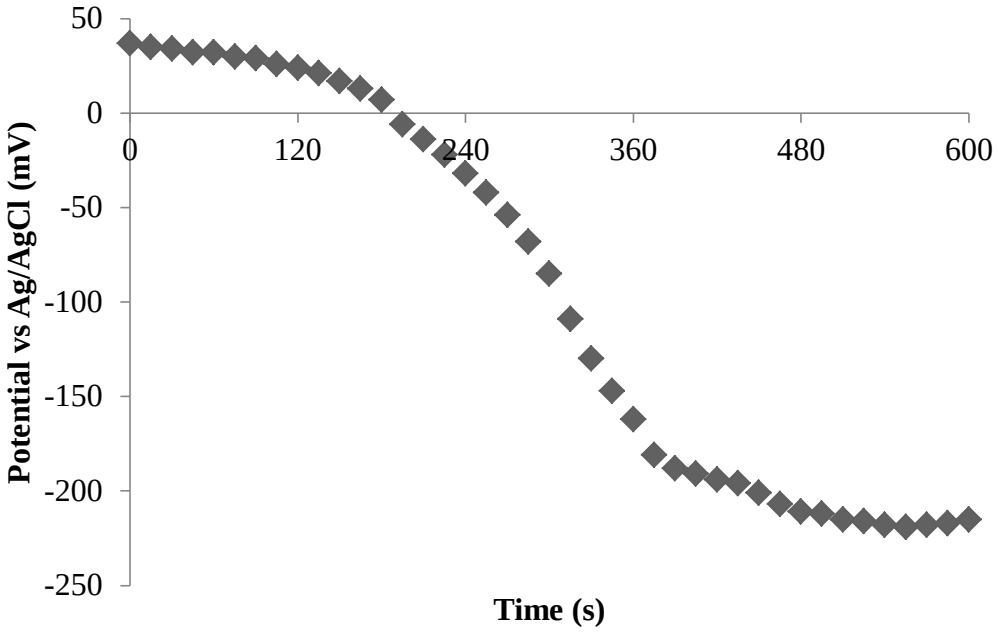

Figure 3.2. Potential over Time of ZrOx Electrodes against Ag/AgCl Reference Electrode in 3M KCl.

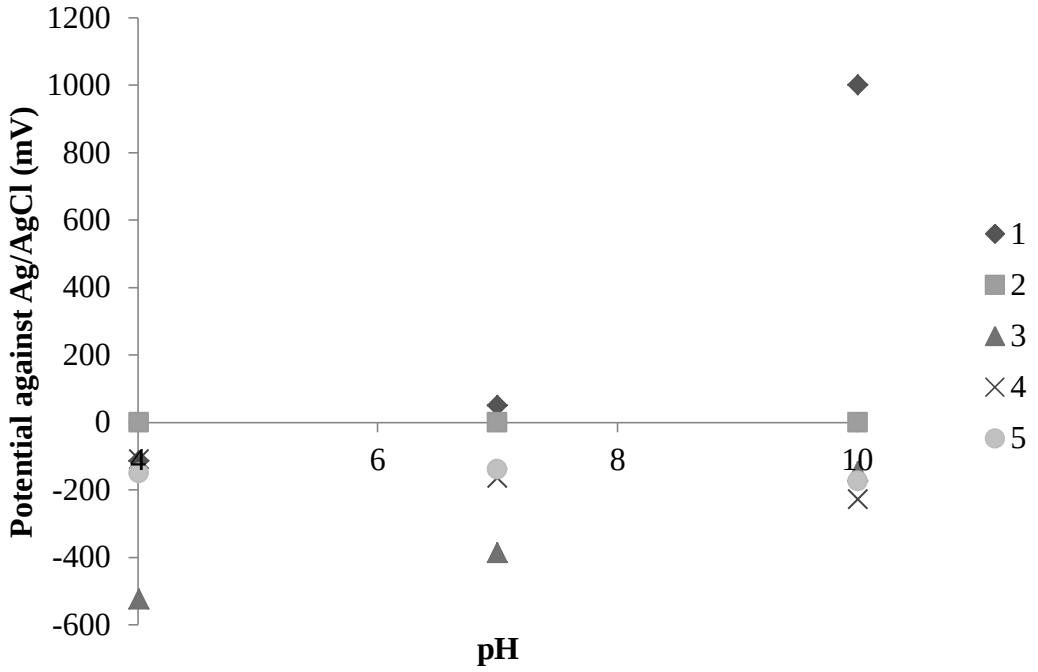

Figure 3.3. ZrOx Potential against Ag/AgCl Reference Electrode in 3M KCl at 25°C in pH calibrations buffers 4.01, 7, and 10.01.

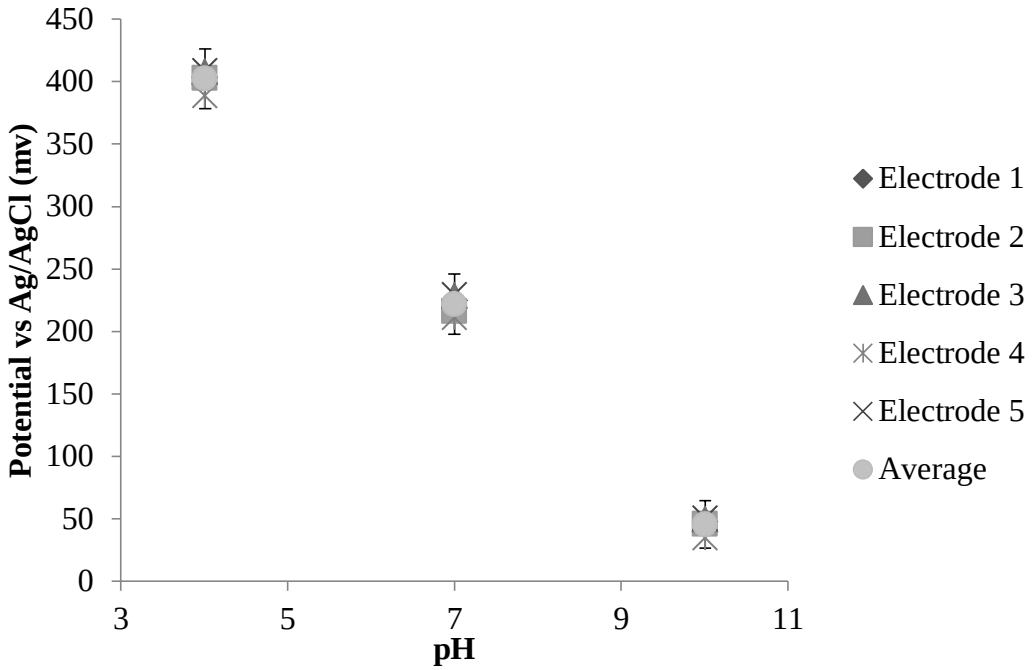

Figure 3.4. Potential of IrOx Electrodes against Ag/AgCl Reference Electrode at 25°C using pH Calibration Buffers 4.01, 7, and 10.01. Error bars represent 3 times the sample standard deviation for each calibration buffer.

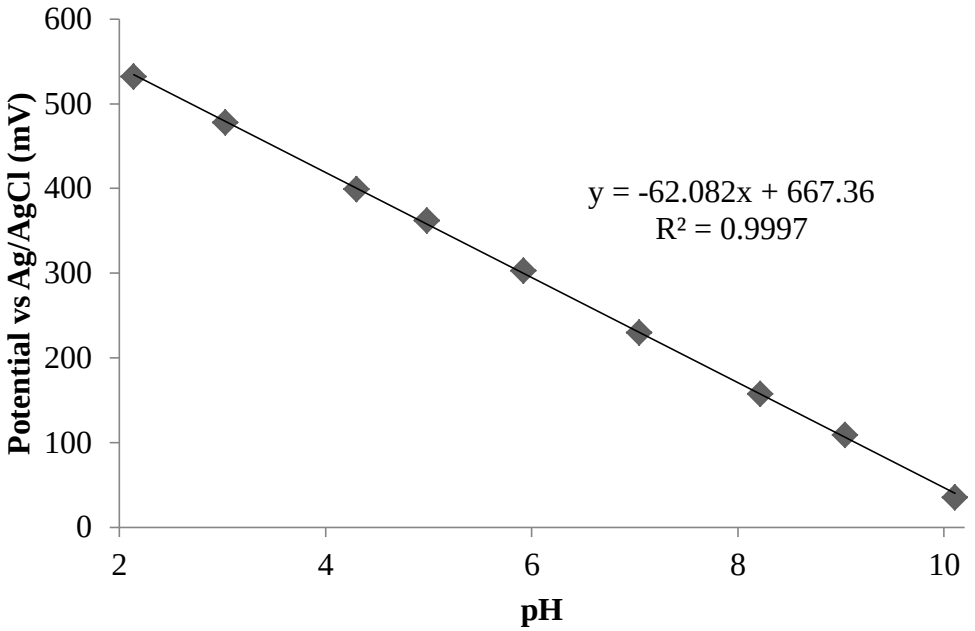

Figure 3.5. Potential of IrOx against Ag/AgCl across pH 2-10 at 25 °C.

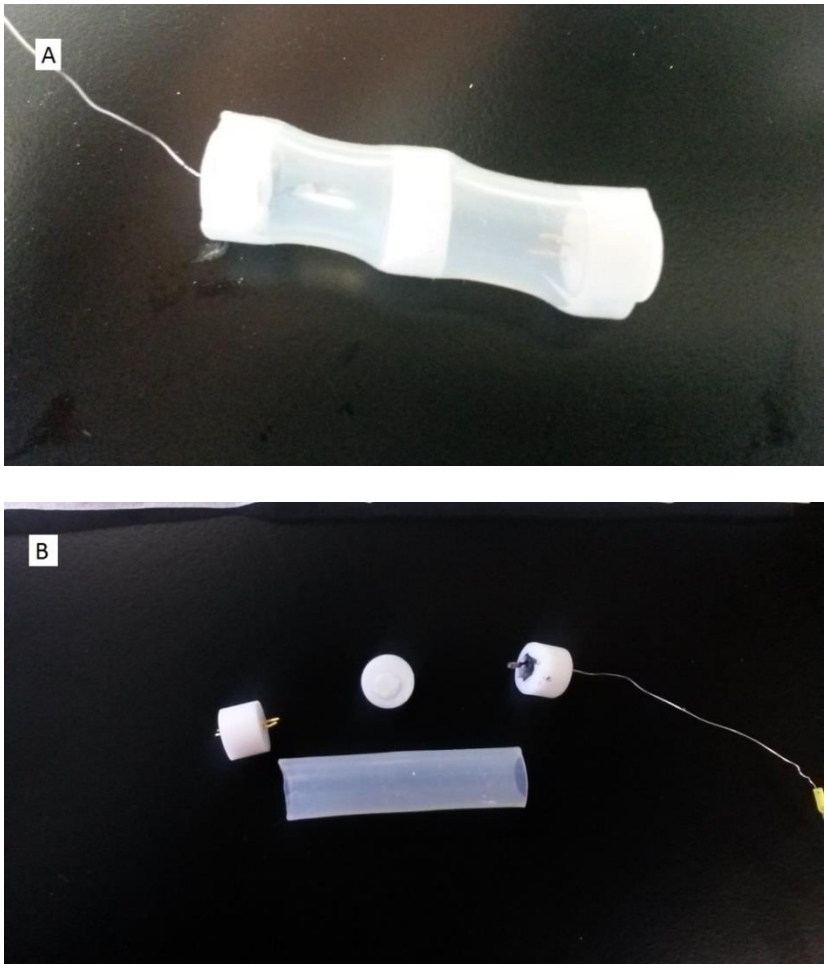

Figure 3.6. First Prototype. (a) cell with end caps and frit holder in place, (b) cell body with end caps and frit holder placed near their respective places, (c) schematic of frit holder.

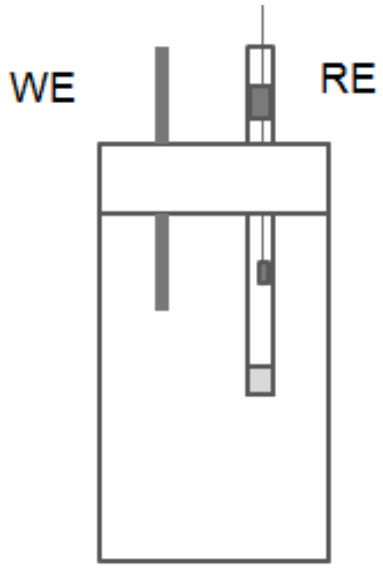

Figure 3.7. Prototype 2.

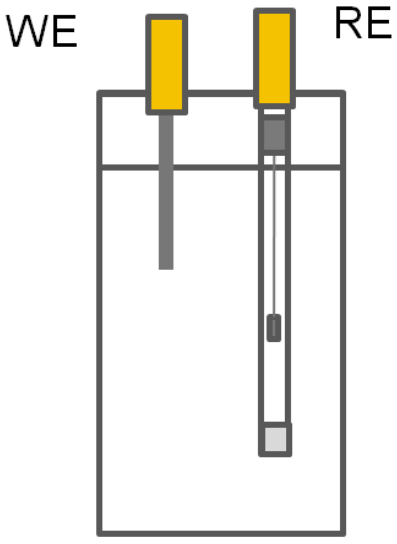

Figure 3.8. Prototype 3.

Figure 3.9. Ag/AgCl Reference Electrode.

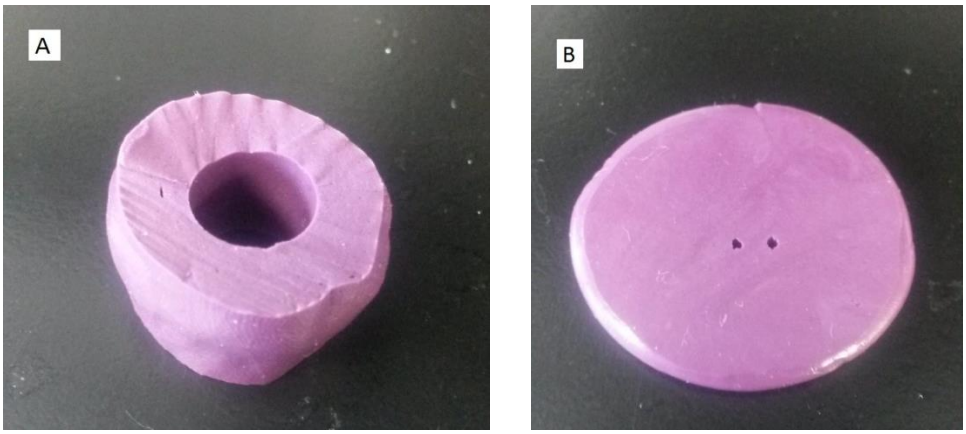

Figure 3.10. Silicone Putty Molds Used for Electrode Cap Production. (a) vertical mold (b) base mold.

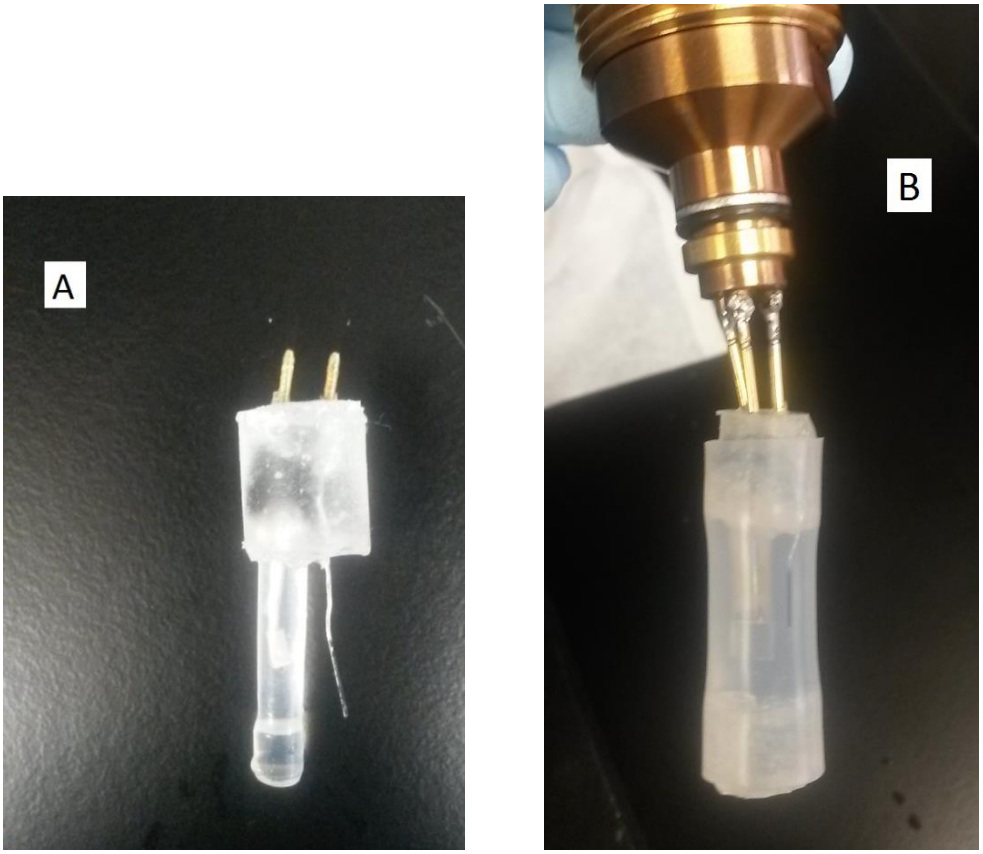

Figure 3.11. Finished prototype. (a) electrode cap (b) completed cell design attached to electrochemical cell lid

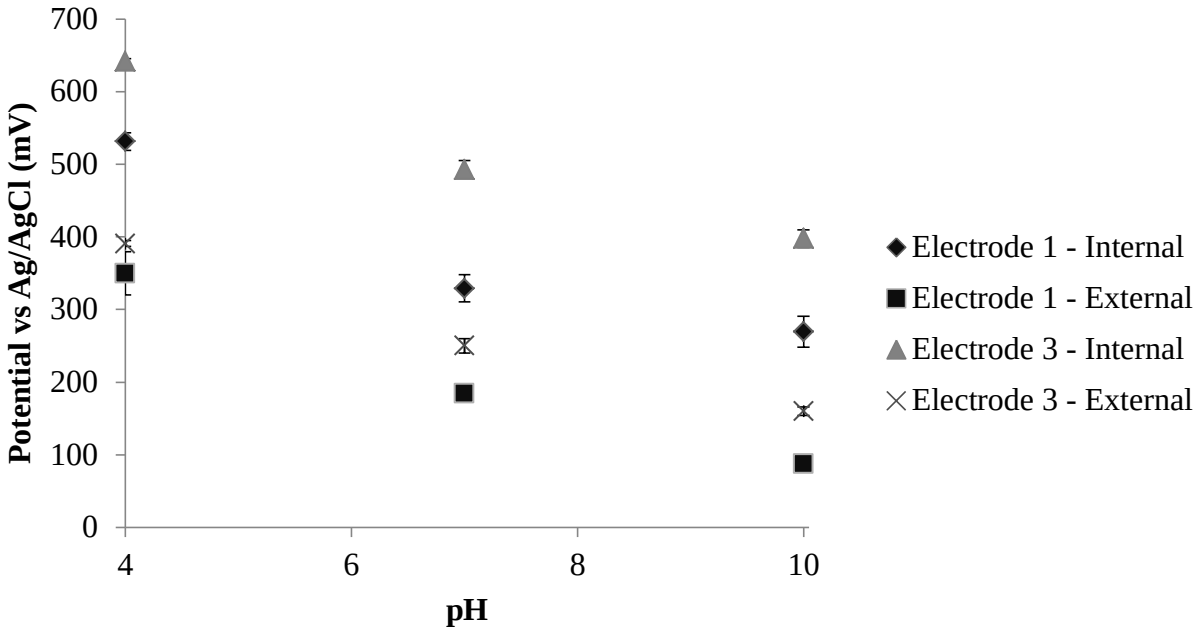

Figure 3.12. Potential of IrOx Electrode vs Internal and External Ag/AgCl Reference Electrode.

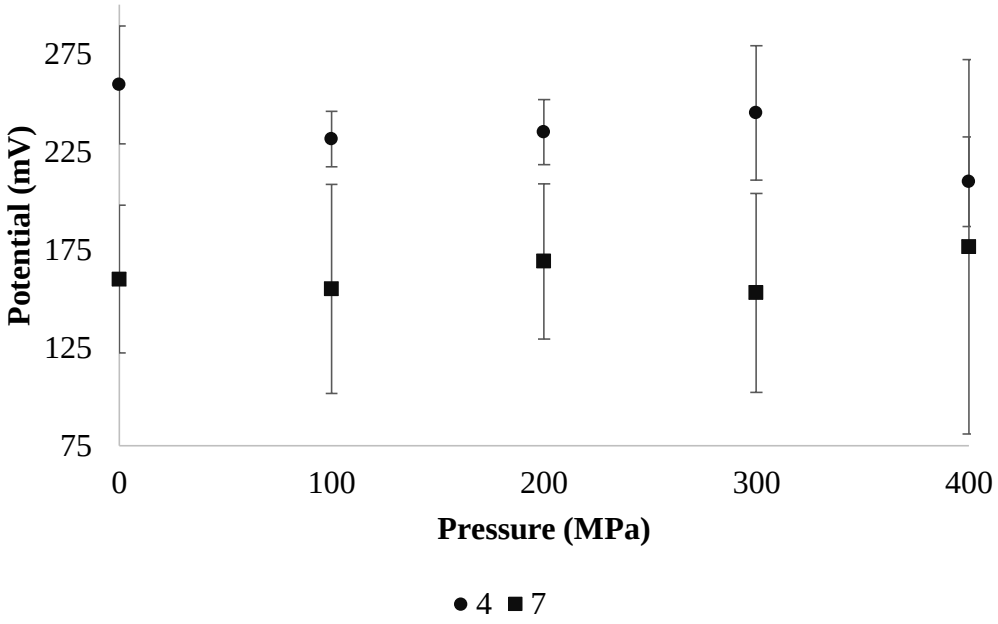

Figure 3.13. Cell Calibration at 25 °C from 0.1 to 400 MPa Using Baroresistant Calibration Buffers. Buffer 7 was pH 7.03 and buffer 4 was 100 mM acetate at pH 4.01.

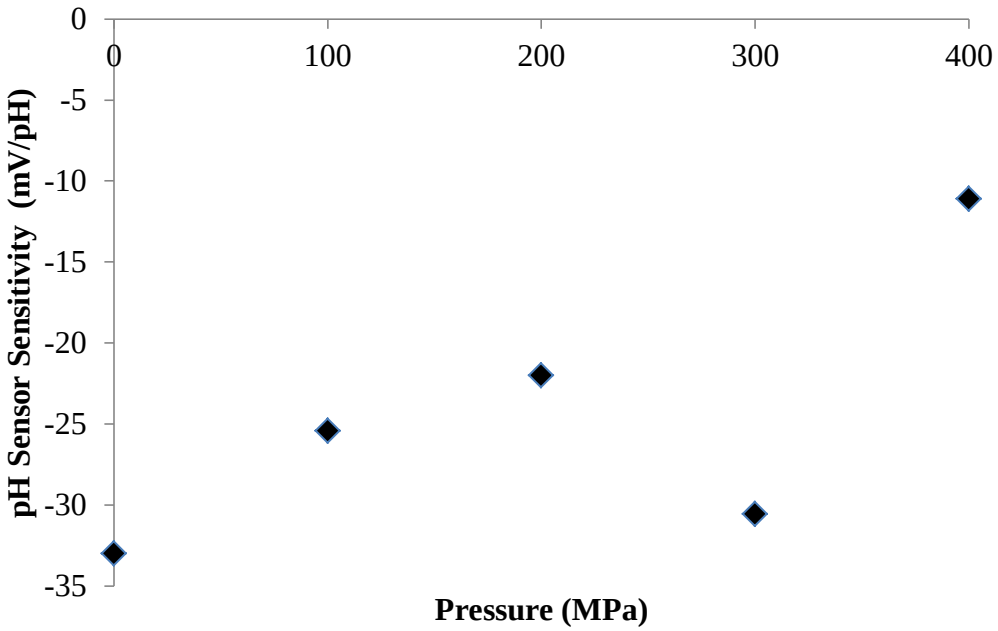

Figure 3.14. pH Sensor Sensitivity vs Pressure.

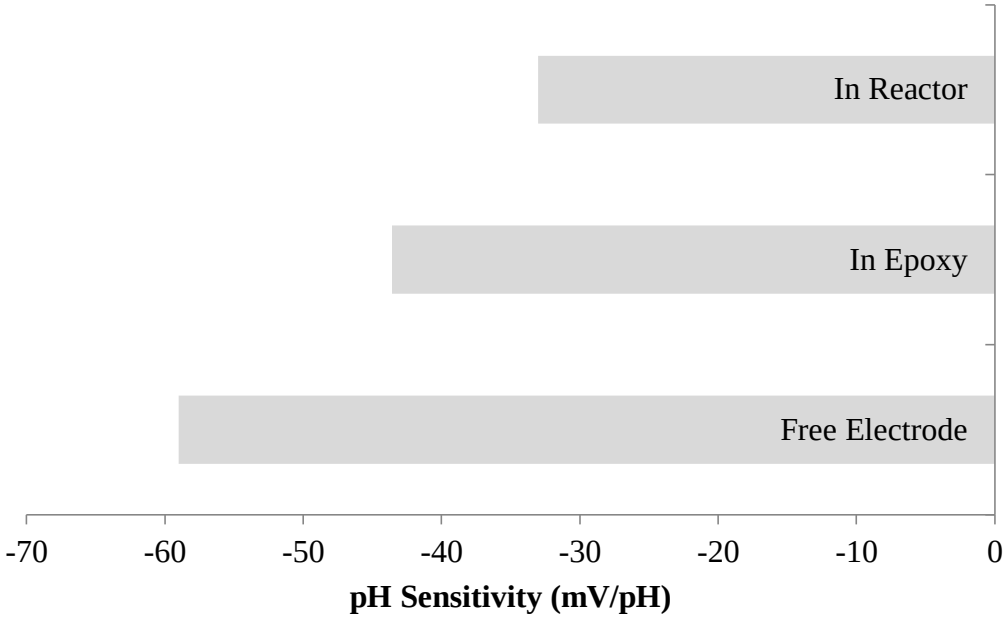

Figure 3.15. Change in pH Sensitivity as Electrodes were Altered.

References

Cruaiies, M.T., Drickamer, H.G., Faulkner, L.R., (1992). Electrochemical Measurements at High Pressure : Solvation and Thermodynamlcs of Electron-Transfer Reactions. 9892(25), 9888-9892.

Elsen, H.A., Monson, C.F., Majda, M., (2009). Effects of electrodeposition conditions and protocol on the properties of iridium oxide pH sensor electrodes. Journal of the electrochemical society 156(1), F1-F6.

Hitchman, M.L., Ramanathan, S., (1988). Evaluation of iridium oxide electrodes formed by potential cycling as pH probes. Analyst 113(1), 35-39.

Kurzweil, P., (2009). Metal Oxides and Ion-Exchanging Surfaces as pH Sensors in Liquids: State-of-the-Art and Outlook. Sensors (Basel) 9(6), 4955-4985.

Lorant, S., Bohnke, C., Roffat, M., Bohnke, O., (2012). New concept of an all-solid-state reference electrode using a film of lithium lanthanum titanium oxide (LLTO). Electrochimica Acta 80, 418-425.

Min, S.K., Samaranayake, C.P., Sastry, S.K., (2011). In situ measurement of reaction volume and calculation of pH of weak acid buffer solutions under high pressure. J Phys Chem B 115(20), 6564-6571.

Pan, Y., Seyfried, W.E., (2008). Experimental and Theoretical Constraints on pH Measurements with an Iridium Oxide Electrode in Aqueous Fluids from 25 to 175 °C and 25 MPa. Journal of Solution Chemistry 37(8), 1051-1062.

Wang, M., Yao, S., Madou, M., (2002). A long-term stable iridium oxide pH electrode. Sensors and Actuators, B: Chemical 81, 313-315.

Zhang, R., Zhang, X., Hu, S., (2010). High temperature and pressure chemical sensors based on Zr/ZrO2 electrode prepared by nanostructured ZrO2 film at Zr wire. Sensors and Actuators B: Chemical 149(1), 143-154.

Zhang, R.H., Zhang, X.T., Hu, S.M., (2008). Zr/ZrO2 sensors for in situ measurement of pH in high-temperature and -pressure aqueous solutions. Analytical Chemistry 80(8), 2982-2987.

Appendix A

CODE FOR MODELING DATA

```
#initial parameters


require(minpack.lm)
colnames(red25) <- c('x', 'y')
y <- red25$y[1:11]
x <- red25$x[1:11]


#trend line production


fit <- nlsLM(y ~ l + (h-l)/((1+q*exp(-b*(8-x)))^(1/v)),
        data = red25,
        start = list(q=.5,
                b=-2,
                v=2,
                h=red25$y[1],
                l=red25$y[11]),
        control = nls.control(tol = 1E-5,
                        minFactor = 1/1024,
                        warnOnly = TRUE))
```

```
t <- coef(fit)[5] +
  (coef(fit)[4]-coef(fit)[5])/((1+coef(fit)[1]*exp(-coef(fit)[2]*(8-x)))^(1/coef(fit)[3]))

#plotting

plot(red25$x, red25$y, xlab = 'pH',
     ylab = 'Ratiometric Absorbance', main =
       'Phenol Red pH-Absorbance Correlation, 25 C',
     xlim = c(5.5,10.5), ylim = c(0,8))
lines(red25$x,t,col = 'gray40', lwd=2)

fit
```